NASA CONTRACTOR REPORT



NASA CR-439

# SIMPLE APPROXIMATIONS FOR FORCE-DEFLECTION CHARACTERISTICS OF AIRCRAFT TIRES

*by Samuel K. Clark*

Prepared under Grant No. NsG-344 *by*
UNIVERSITY OF MICHIGAN
Ann Arbor, Mich.
*for*

NATIONAL AERONAUTICS AND SPACE ADMINISTRATION - WASHINGTON, D. C. - MAY 1966

NASA CR-439

# SIMPLE APPROXIMATIONS FOR FORCE-DEFLECTION CHARACTERISTICS OF AIRCRAFT TIRES

By Samuel K. Clark



Prepared under Grant No. NsG-344 by
UNIVERSITY OF MICHIGAN
Ann Arbor, Mich.

for

NATIONAL AERONAUTICS AND SPACE ADMINISTRATION

For sale by the Clearinghouse for Federal Scientific and Technical Information
Springfield, Virginia 22151 – Price $3.00

## ACKNOWLEDGMENTS

The support of the National Aeronautics and Space Administration made this work possible, and is gratefully acknowledged, as is their permission to reproduce their earlier experimental data.

TABLE OF CONTENTS

# LIST OF ILLUSTRATIONS

LIST OF ILLUSTRATIONS (Concluded)

## NOMENCLATURE

### English Letters

| | |
|---|---|
| b | Minor diameter of contact patch ellipse, in. |
| d | Tire diameter measured to carcass centerline, in. |
| H | Tire section height from bead to carcass centerline, in. |
| $K_L$ | Elastic spring constant for lateral tread distortion, psi |
| L | Major diameter of contact patch ellipse, in. |
| M | Torsional moment, in. lb |
| O | Bead centerline point |
| P | Vertical load, lb |
| $p_o$ | Inflation pressure, psi |
| Q | Tire side force, lb |
| $r_1$ | Section radius of curvature, in. |
| S | Tire side force, lb |
| T | Tire running band tension, lb |
| $\omega$ | Running band lateral deflection, in. |
| w | Section width, in. |
| x | Position along circumference of tire, in. |

### Greek Letters

| | |
|---|---|
| $\alpha$ | Angle of lateral deflection |
| $\beta$ | Included half angle in minor diameter of contact patch ellipse |
| $\Delta_H$ | Lateral or side deflection of tire, in. |

Greek Letters

| | |
|---|---|
| $\Delta_V$ | Vertical deflection of tire, in. |
| $\Delta_T$ | Lateral deflection at end of contact patch during twisting deformation, in. |
| $\lambda$ | $\sqrt{K_L T}$ |
| $\eta$ | An arbitrary or experimentally determined reduction factor to account for contact patch distortion during tire twist, dimensionless |
| $\varphi$ | Angle of twist of tire |
| $\theta$ | Included half angle in major diameter of contact patch ellipse |

## SUMMARY

Simplified expressions are derived for three of the more commonly used force-deflection characteristics of aircraft tires in terms of tire size and inflation pressure. These are the vertical load-vertical deflection, side load-side deflection and torsional moment-angle of twist relationships. The derivations are based on the concept of treating the tire as a pressurized torus of circular cross-section with no bending rigidity, and on the concept of treating the outer portion of the tire, or "running band" as a string on an elastic foundation. Predictions from such simplified theories are compared with extensive experimental data obtained by N.A.C.A. in 1953, and agreement is generally good although far from perfect.

The primary usefulness of such expressions probably lies in the area of preliminary design, where extensive parametric studies are often required to optimize response under many different input conditions. They may also be of use in ground vibration studies of aircraft.

## ANALYSIS

During deformation of a pneumatic tire two kinds of forces act. The first of these is set up by bending of the tire carcass, while the second comes about due to deformation of the carcass walls, which themselves carry large membrane forces due to inflation pressure. In an aircraft tire the latter type of force is predominant in many situations because the aircraft tire usually operates at a rather high inflation pressure, so that these membrane forces are much larger than those generated by carcass bending.

Examination of toroidal shell equilibrium conditions shows that to a great extent the membrane forces due to inflation are statically determinate and can be calculated, or at least estimated, independently of tire structure or wall thickness. This leads to the conclusion that tire load-deflection relations which depend primarily on membrane forces might very well be calculated analytically. Of course, such calculations would not be valid for cases where the inflation pressure became small enough so that membrane effects were small compared to bending.

Examination of the forces involved in tire deformations showed that three common cases might be treated by such an approach:

a. Vertical load-vertical deflection relations
b. Side load-side deflection relations
c. Torsional moment-angle of twist relations.

In all of these it is felt that inflation causes membrane forces which in turn cause the major part of the spring-deflection relation.

Considerable use has been made of models for predicting the steering characteristics of pneumatic tires. The most widely used of these models have been the string on the elastic foundation and the beam on the elastic foundation. In both of these the tread region is imagined to be the string or beam, while the sidewall region makes up the elastic foundation. One of the shortcomings of such models has been the difficulty of estimating the magnitude of the elastic foundation constant. A method for overcoming this difficulty is presented in this report.

Perhaps the most common spring characteristic of a pneumatic aircraft tire is its vertical deflection under load. This deformation process may be approximated in a very rough way by a geometric calculation of the contact area of a tire with a flat surface. Referring to Fig. 1, which is a side view

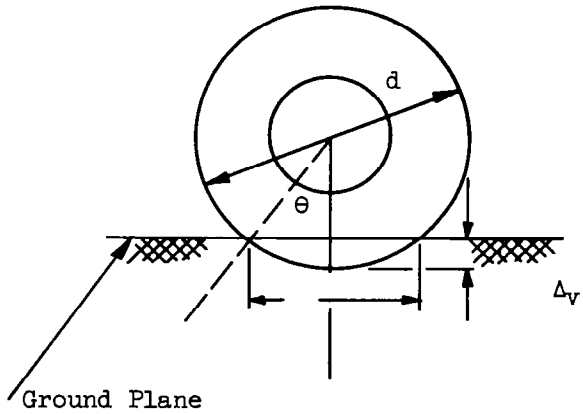


Fig. 1. Side view of deformed tire.

of a tire, it is seen that the vertical deflection $\Delta_V$ and contact patch length L are related by the parameter $\theta$:

$$\Delta_V = \frac{d}{2}(1-\cos\theta) \qquad (1)$$

$$\frac{L}{d} \simeq \sin\theta \qquad (2)$$

For relatively small deflections $\Delta_V$ compared with diameter d, one may write

$$\Delta_V \simeq \frac{\theta^2}{2} \cdot \frac{d}{2} \qquad (1)'$$

$$\frac{L}{d} \simeq \theta \qquad (2)'$$

from which

$$\Delta_V \simeq \frac{L^2}{4d} * \qquad (3)$$

Aircraft tires are typically molded without the heavy, buttress-like shoulder structure used in automotive and truck tires. Their cross-sectional shape is closer to a circle. On this basis, relations similar to Eqs. (1), (2) and (3) may be developed for a cross-section of a typical aircraft tire, as shown in Fig. 2. Here, the vertical deflection and contact patch width

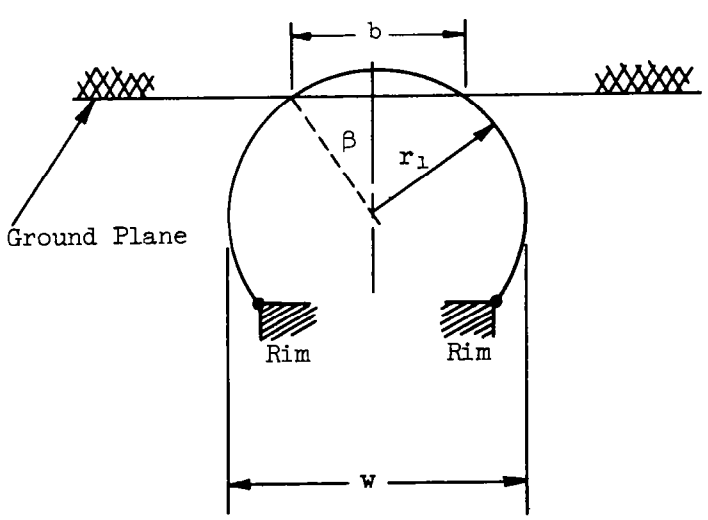


Fig. 2. Cross section of aircraft tire.

*Tests and more refined mathematical models both show that the contact patch length is only 75% to 85% of the geometric intersection length used here. This will be disregarded in these approximations.

are related through the parameter $\beta$:

$$\Delta_v = r_1(1-\cos\beta) \tag{4}$$

$$\frac{b}{2r_1} \simeq \sin\beta \tag{5}$$

If $\Delta_v$ is small compared with $r_1$, Eqs. (4) and (5) may be simplified and combined as before to give

$$\Delta_v \simeq r_1 \frac{\beta^2}{2} \tag{4}'$$

$$\frac{b}{2r_1} \simeq \beta \tag{5}'$$

and

$$\Delta_v = \frac{b^2}{8r_1} \tag{6}$$

Next, one may note that an aircraft tire is usually rather highly inflated. The shell membrane effects become important compared with the shell bending effects. Under these circumstances the tire shape approximates, but does not reach, a circle. Hence one further approximation may be made relating the section width w of Fig. 2 to the radius of curvature $r_1$ in the form

$$r_1 \simeq \frac{w}{2} \tag{7}$$

and combining this with Eq. (6) gives

$$\Delta_v \simeq \frac{b^2}{4w} \tag{8}$$

The length of the contact patch is obtainable from Eq. (3), and its width from Eq. (8). Tests show that the contact patch in a tire of typical aircraft construction is approximately elliptical in shape with a pressure distribution which varies but whose average value is close to the inflation

pressure $p_o$. Hence, the vertical load P may be approximated by

$$P \simeq \pi \frac{L}{2} \frac{b}{2} p_o \quad \text{or}$$

$$\boxed{P \simeq \pi\, p_o\, \Delta_v \sqrt{dw}} \tag{9}$$

This gives a relation between total vertical load, inflation pressure $p_o$ and deflection $\Delta_v$ such that

(a) Load P is directly proportional to deflection $\Delta_v$ and to inflation pressure $p_o$

(b) Load P is directly proportional to the carcass section width w and tire diameter d, each to the one-half power.

Another important property of a pneumatic aircraft tire is its lateral, or side, force-deflection relation. This particular elastic characteristic has had extensive treatment in the literature since it is closely related to the cornering force developed by a tire while running at a slip angle. Discussions of some aspects of the lateral stiffness have been given by Andrews,[1] Saito[2] and Rotta.[3] A review of much of this work is given in the excellent summary of Frank.[4] There, it was concluded that for tires of radial or belted construction, or for tires with very heavy tread sections, the beam on the elastic foundation is probably the best model. For tires of bias ply construction, such as an aircraft tire, the string on the elastic foundation gives good results, and that type of model will be adopted here.

It is first necessary to develop a means of relating the tire parameters to the lateral elastic foundation modulus, or stiffness, required in the theory of a string on an elastic foundation. In order to do this the tire cross-section will be idealized rather drastically, as shown in Fig. 3a and 3b.

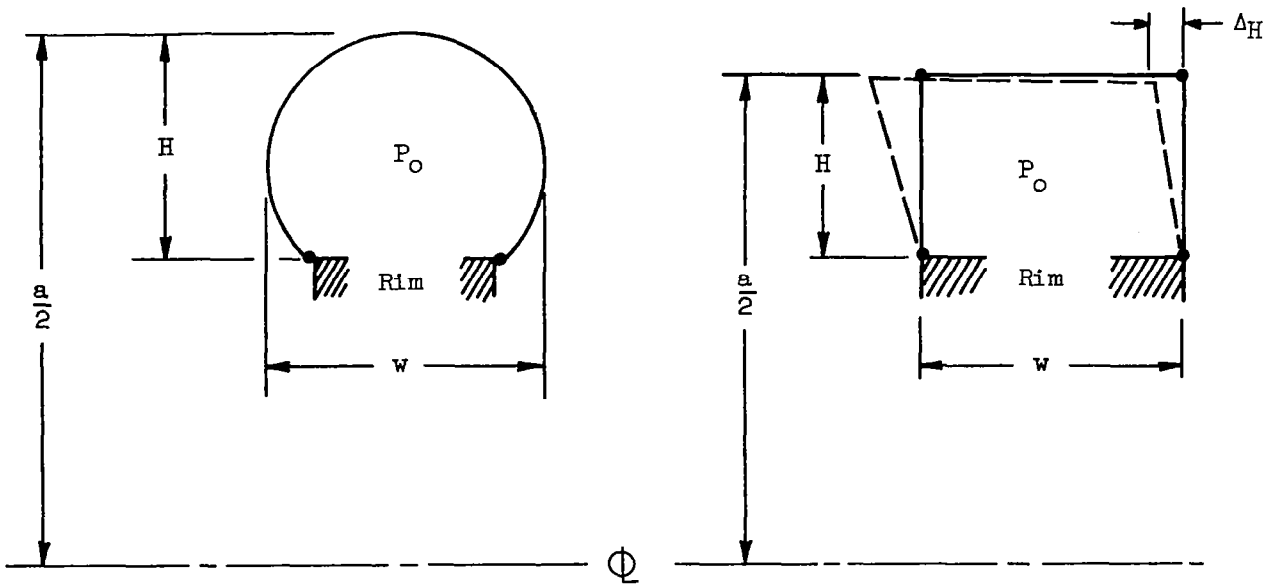


Fig. 3. Idealized section of aircraft tire.

The assumed lateral deflection $\Delta_H$ is shown by the dashed lines of Fig. 3b. If a unit width of the tire, as shown in Fig. 3b is considered a pin-jointed structure, then it may be analyzed in its assumed deformed condition as shown in Fig. 4, under the action of inflation pressure $p_o$ and an assumed side force Q.

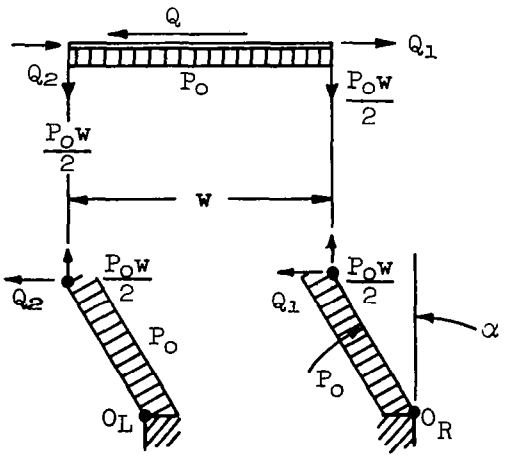


Fig. 4. Free body diagram of deformed tire.

For the right hand sidewall, taking moments about $O_R$ gives

$$Q_1 H \cos \alpha = \frac{p_o w}{2} H \sin \alpha + p_o H \cdot \frac{H}{2}$$

For small $\alpha$,

$$Q_1 \simeq p_o \frac{H}{2} + p_o \frac{w}{2} \frac{\Delta_H}{H} \tag{10}$$

For the left hand sidewall, taking moments about $O_L$ gives

$$-Q_2 H \cos \alpha + \frac{p_o w}{2} H \sin \alpha = p_o H \cdot \frac{H}{2}$$

$$-Q_2 \simeq p_o \frac{H}{2} - p_o \frac{w}{2} \frac{\Delta_H}{H} \tag{11}$$

The total side force Q is given by

$$Q = Q_1 + Q_2 = p_o \frac{w \Delta_H}{H}$$

$$Q/\Delta_H = \frac{p_o w}{H} = K_L, \tag{12}$$

where $K_L$ is a lateral foundation modulus for the string. The string itself may be visualized as the upper portion of the pin-jointed truss approximation of Fig. 4. This band of width w may be assumed to carry the entire pressure load. From conventional pressure vessel theory, the band tension T is given by

$$T = w p_o \frac{d}{2} \tag{13}$$

It is difficult to check either the lateral spring rate $K_L$ or the band tension T, as given by Eqs. (12) and (13), directly. For example, Thorsen[5] obtains for the lateral spring rate $K_L$ the expression given in Eq. (12) multiplied by $\pi/4$, while Stevens[6] introduces a weighted band tension proportional to the distance from the rim. Some clarification of the general accuracy of

Eqs. (12) and (13) can be obtained by a simple experiment in which a tire of negligible carcass stiffness is loaded laterally at a point. The string on the elastic foundation may be used as a basic model for the force-deflection relation.

The equation of static equilibrium for the string on elastic foundation is

$$T \frac{d^2u}{dx^2} - K_L u = 0 \tag{14}$$

from which, letting $\lambda^2 = K_L/T$

$$u = Ae^{-\lambda x} + Be^{\lambda x} . \tag{15}$$

Considering the tire diameter large compared with the patch length, one obtains B = 0 from which

$$u = Ae^{-\lambda x}$$

But $(u)_{x=0} = \Delta_H$ is a boundary condition, so that

$$u = \Delta_H e^{-\lambda x} \tag{16}$$

$$\frac{du}{dx} = \text{Slope} = \Delta_H \lambda e^{-\lambda x} \tag{17}$$

and the force component perpendicular to the string is given by

$$S = 2T\left(\frac{\partial u}{\partial x}\right)_{x=0}$$

as shown in Fig. 5. Using Eqs. (13) and (17),

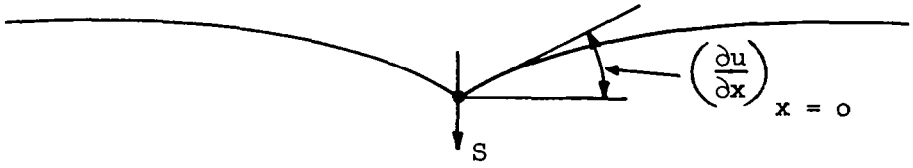


Fig. 5. String under point load.

one obtains

$$S = \sqrt{2}\, \Delta_H\, p_o\, w \sqrt{\frac{d}{H}} \tag{18}$$

for a concentrated load.

Experiments were conducted on a tire in which both the tread and much of the carcass had been stripped away, leaving a thin web or network of cords. This is shown in Fig. 6.

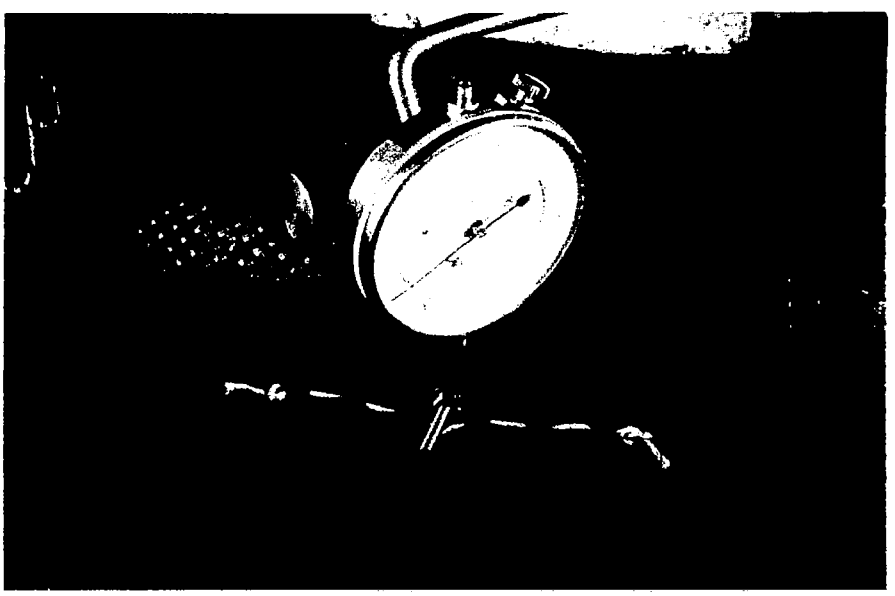

Fig. 6. Tire with negligible bending stiffness and point load.

In this same photograph a short length of twisted steel cable may be seen, to which a small weight-pan is wired. In addition, a bolt is firmly attached to the web of the carcass and acts as a reference point for the dial gauge.

Figure 7 shows a somewhat larger overall view of this tire in the loaded condition. In spite of the length of cable used, the load is applied in almost a concentrated fashion. The measured spring rate may be compared with

Fig. 7. Loaded tire with negligible bending stiffness.

that given by Eq. (18), and the results are given below in Table I.

TABLE I

| Inflation Pressure psi | 5 | 9 | 13 |
|---|---|---|---|
| Measured Spring Rate lbs/in | 161 | 234 | 334 |
| Calculated Spring Rate lbs/in | 108 | 195 | 280 |

While calculations and measurement do not agree very well here, they at least indicate that the lateral spring rate should probably not be reduced below the value given by Eq. (12), and that the effective band tension should probably not be reduced below the value given by Eq. (13), since in either event the calculated values would deviate even more from the measured ones. Recognizing that Eqs. (12) and (13) are relatively crude expressions anyway, they will be retained in that form without further modification.

The concept of the string on the elastic foundation may be extended to represent the contact patch of a tire under lateral or side load. Ideally, the contact patch mid-line may be visualized as a straight line segment which is laterally displaced from the equilibrium position, as shown in Fig. 8.

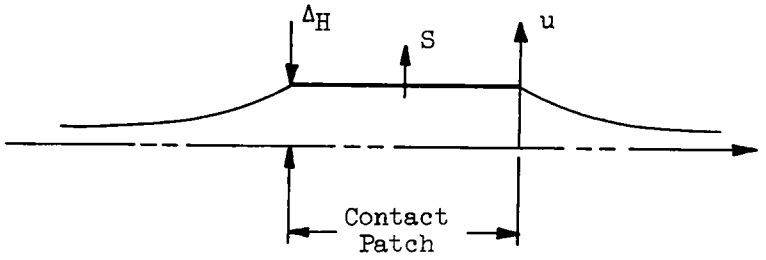


Fig. 8. Idealized contact patch under lateral deflection.

In actuality the contact patch is not displaced in this way. Instead, the straight line segment is curved. This can be demonstrated clearly by loading and then laterally displacing a small inflated inner tube pressed against a Plexiglass plate, as shown in the photograph of Fig. 9. The center line of the distorted tube may be clearly seen to follow a curved path, and since the relation between force and tire deflection involves the reduced deflections at the end of the contact area, it is necessary to take these into account in subsequent

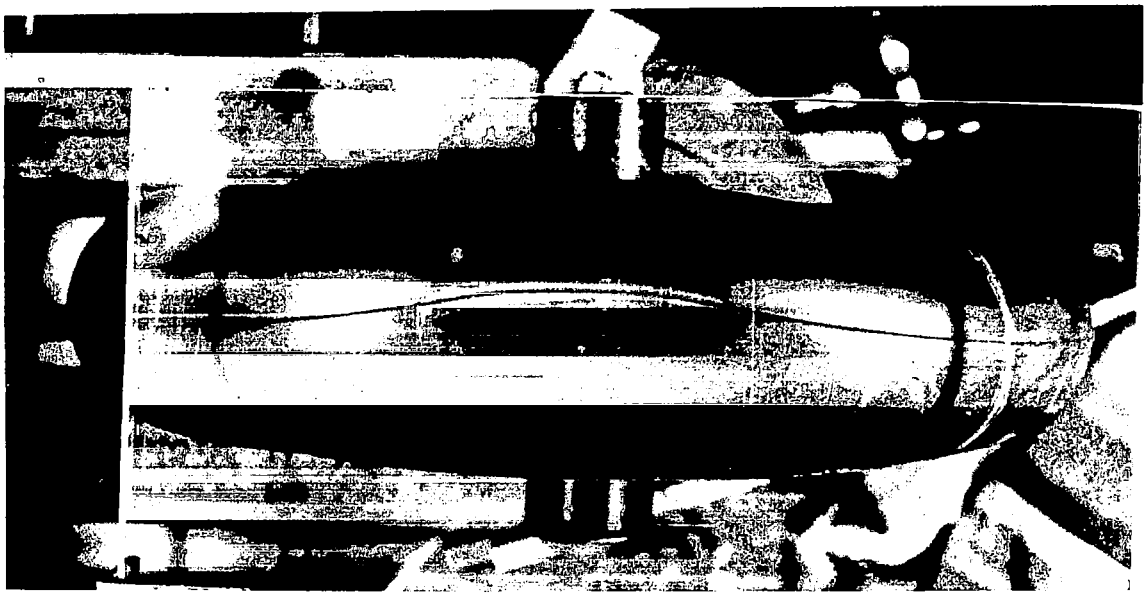

Fig. 9. Laterally displaced loaded inner tube.

calculations. For this reason we adopt the distorted contact patch shown in Fig. 10 as a model, and introduce the reduction factor $\eta$ to account for the displacement of the ends relative to the center. Later on $\eta$ will be given a

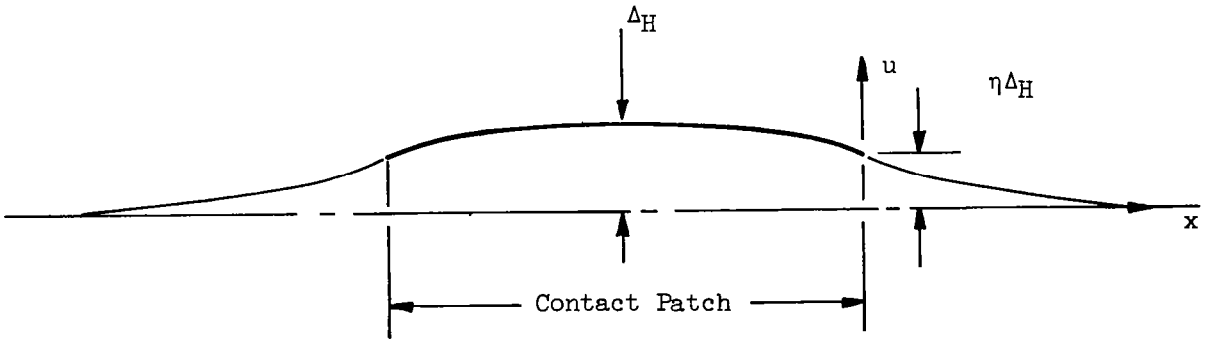


Fig. 10. Assumed contact patch form for lateral deflection.

numerical value.

In the contact patch region the pressure of contact just balances the vertical reactions caused by inflation which act on the sidewalls, shown in

Fig. 4, provided that one continues to assume a uniform pressure distribution $p_o$ over the contact patch. Since these vertical reactions are the forces which help generate the lateral spring rate, their absence means that no lateral spring rate acts against the tread band shown in Fig. 10 inside the contact patch length. It is only outside of this length that such forces act to restrain the string under tension. This leads to the idea that the lateral force may be obtained by computing the restoring tension forces acting on the contact patch area, and that these tension forces are obtainable from string theory. A sketch of the loaded contact patch is given in Fig. 11,

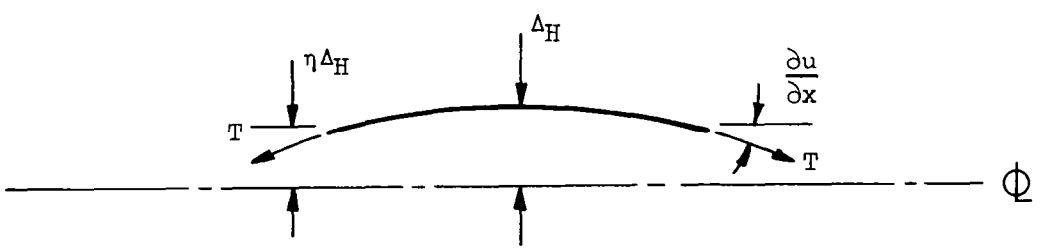


Fig. 11. Forces acting on the contact patch.

from which the total restoring force component perpendicular to the centerline is given by

$$S = 2\,T\left(\frac{\partial u}{\partial x}\right)_{x=0} = 2\,\eta\,\Delta_H\sqrt{K_L T}$$

Using Eqs. (12) and (13), and calling the side force S, gives

$$\boxed{S = \sqrt{2}\,\Delta_H\,p_o\,\eta w\sqrt{\frac{d}{H}}} \qquad (19)$$

From this expression, lateral spring rate may be obtained directly. It is seen that side force S is

(a) Linearly proportional to side deflection $\Delta_H$

(b) Linearly proportional to inflation pressure $p_o$ and to section width w

(c) Proportional to the one-half power of a dimensionless shape factor which is the ratio of tire diameter d to section height H.

(d) Independent of vertical load or contact patch length.

The concept of the "running band" as a string on an elastic foundation is also useful in defining the torsional stiffness of an aircraft tire under a twisting couple about an axis perpendicular to the ground plane and passing through the wheel centerline. Referring to Fig. 12, it is seen that the band tensions ideally act to form a couple about the contact patch- center-point. Again, however,

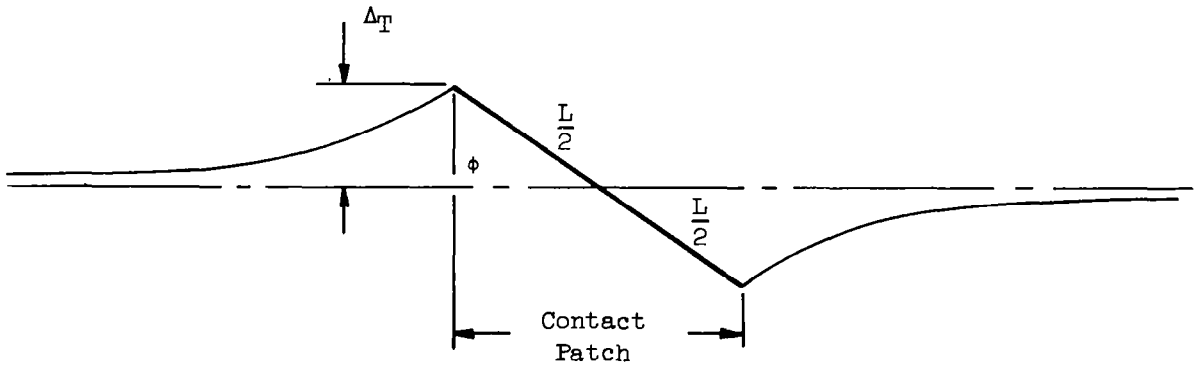


Fig. 12. Idealized contact patch under twist.

a real tire does not act in this ideal way. Figure 13 is a photograph of the same inner tube used in Fig. 9, but now distorted by twisting about a central axis. This shows the curvature of the contact patch, and again leads to the concept of reducing the deflection $\Delta_T$ of the contact patch extremity by an

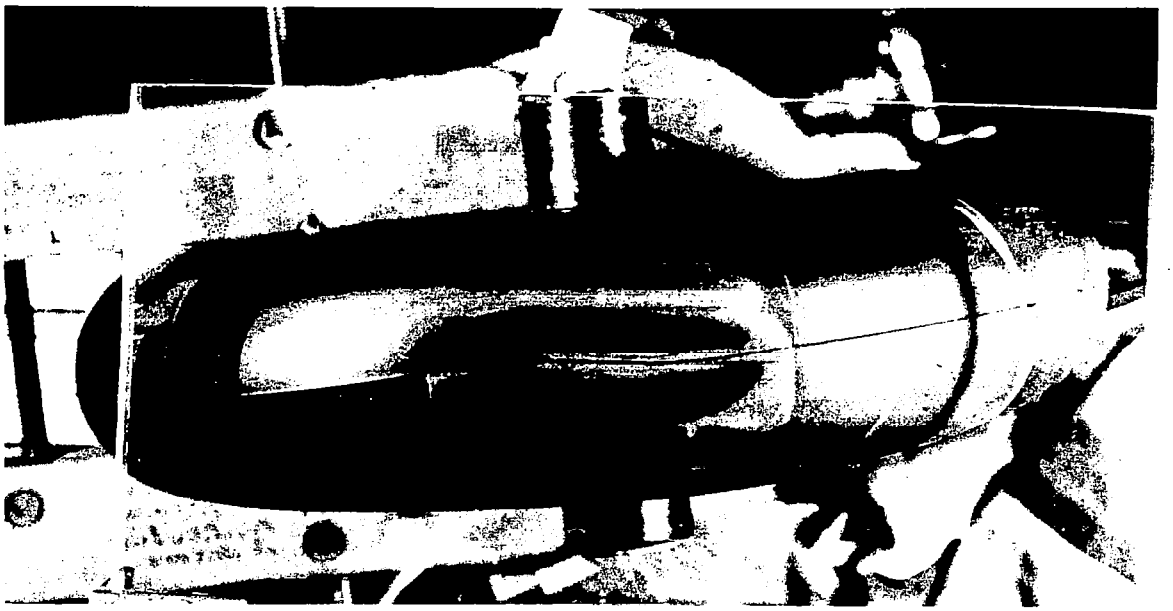

Fig. 13. Twisted loaded inner tube.

amount $\eta$. This is illustrated by the sketch of Fig. 14.

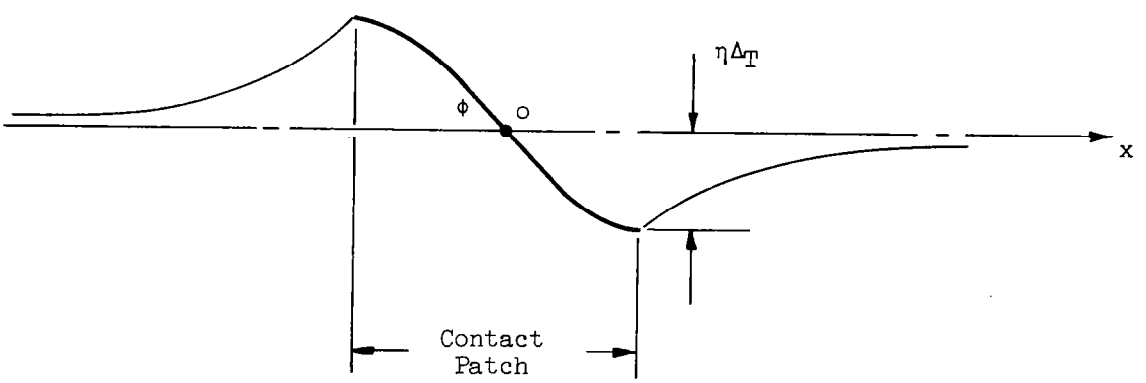


Fig. 14. Assumed contact patch form for twist.

Using this factor, and the previous values of string tension and slope, one may write an expression for the moment about point O as

$$M = 2\eta\Delta_T \sqrt{K_L T} \cdot \frac{L}{2} \quad . \tag{20}$$

Using this, and Eqs. (12) and (13), one may write

$$M = \varphi \frac{L^2}{2\sqrt{2}} p_o \, w \sqrt{\frac{d}{H}} \eta \tag{21}$$

where $\Delta_T = \eta \frac{L}{2} \varphi$, with $\eta$ as a reduction factor for deflection. Recalling that $L^2 = 4d \, \Delta_V$ and $P = \pi \, \Delta_V \, p_o \sqrt{d r_1}$, one obtains, using $r_1 \simeq w/2$,

$$\boxed{\frac{M}{\varphi} = \eta \left(\frac{\sqrt{2}}{\pi}\right) d \, P \sqrt{\frac{w}{H}}} \tag{22}$$

This leads to the interesting conclusions that torsional moment is

(a) Linearly proportional to angle of twist $\phi$.

(b) Linearly proportional to tire diameter d and to tire vertical load P.

(c) Proportional to the square root of a dimensionless tire shape factor w/H, section width over section height.

(d) Independent of inflation pressure $p_o$.

## COMPARISON OF THEORY WITH EXPERIMENT

The expressions given in Eqs. (9), (19) and (22) are only of superficial interest unless they agree with experiment. It is extremely fortunate that extensive experiments on aircraft tires have been reported by W. B. Horne,[7] of the National Aeronautics and Space Administration. The expressions derived here are compared to the data given by Horne by means of superimposing heavy solid lines representing theory upon his original plots. These are shown in Figs. 15 through 32. In making these, measurements taken on Fig. 9 showed that the reduced deflection factor $\eta$ should be chosen numerically to be approximately

$$\eta \simeq 0.75$$

and this has been followed in these plots.

The tires tested by Horne are shown in cross-section in Fig. 15 and photographs are given in Fig. 16. The pertinent dimensions

$w$ = Section width

$H$ = Section Height

$d$ = Tire diameter

are estimated from Fig. 15 by measuring to the assumed location of the tire carcass mid-line, which is the neutral axis in bending of the tire and is the centroid for the membrane forces. These dimensions are listed in Table 2.

TABLE II

TIRE SECTION DIMENSIONS IN INCHES

| Tire | A | B | C | D | E |
|---|---|---|---|---|---|
| w | 12 | 14 | 12 | 12 | 8 |
| H | 12 | 12 | 11 | 10 | 6 |
| d | 54 | 54 | 44 | 44 | 28 |

Comparison of theory with experiment for vertical load-deflection curves shows that generally Eq. (9) gives results slightly higher than experiment. However, the slopes of load deflection curves appear to be very close to experiment, and for this reason Eq. (9) may be useful in ground vibration studies where the rate is more important than the actual value.

Similar comparisons with lateral force-deflection data and Eq. (19) shows that, on the average, predictions of side force are within the range of experimental data for cases where the inflation pressure is relatively high. This is because the membrane-induced lateral stiffness component is the primary one in this condition. In cases where the inflation pressure is low, the predictions of Eq. (19) tend to be somewhat lower than the measured data. This seems reasonable, since at low pressures the bending rigidity of the tire carcass becomes, relative to the membrane-induced rigidity, a more important factor, and this is not taken into account in this analysis.

Torsional load deflection curves show even more hysteresis than do the side deflection curves. It is difficult to assign any specific torsional spring rate to a given set of conditions. In many cases the predictions of Eq. (22) are well within the hysteresis loop, particularly at the larger

vertical loads. At low vertical loads agreement between measured data and experiment is not as good in most cases, although it is difficult to generalize here. It is probable that Eq. (22) would be suitable for some preliminary design purposes.

## REFERENCES


1. Andrews, H., "A Discussion of the Lateral Force and Moment Characteristics of Pneumatic Tires," Cornell Aeronautical Laboratory Report TB-902-F-1, Feb. 1954.

2. Saito, Y., "A Study of Dynamic Steering Properties of Pneumatic Tires," Ninth International Automobile Technical Congress, 1962.

3. Rotta, J., "Zur Statik des Luftreifens," Ingenieur-Archiv, v. 17, (1949), p. 129-141.

4. Frank, F., "Grundlagen zur Berechnung der Seitenführungs Kennlinien von Reifen," Kautschuk und Gummi. Kunststoffe, 8, 515-533 (1965).

5. Thorsen, K. R., "A Rational Method for Predicting Tire Cornering Forces and Lateral Stiffness," Boeing Airplane Company Report No. D-11719, March, 1951.

6. Stevens, J. E., "Relaxation Characteristics of Pneumatic Tires," Jour. Aero/Space Sciences, June 1959, p. 343-350.

7. Horne, Walter B., "Static Force-Deflection Characteristics of Six Aircraft Tires under Combined Loading," N.A.C.A. Technical Note 2926, National Advisory Committee for Aeronautics, Washington, D. C. May 1953.

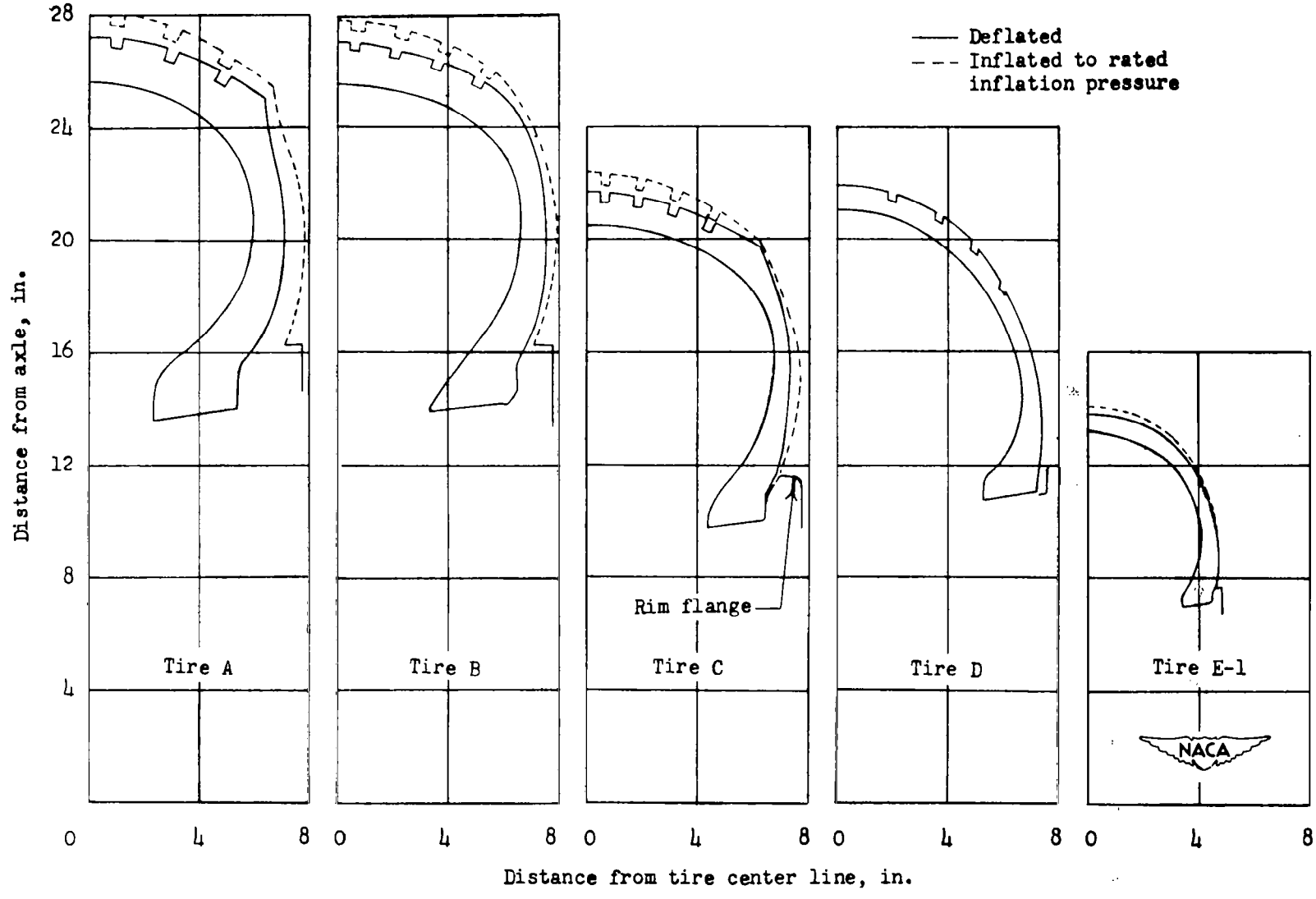


Fig. 15. Dimensions of test tires from NACA TN 2926

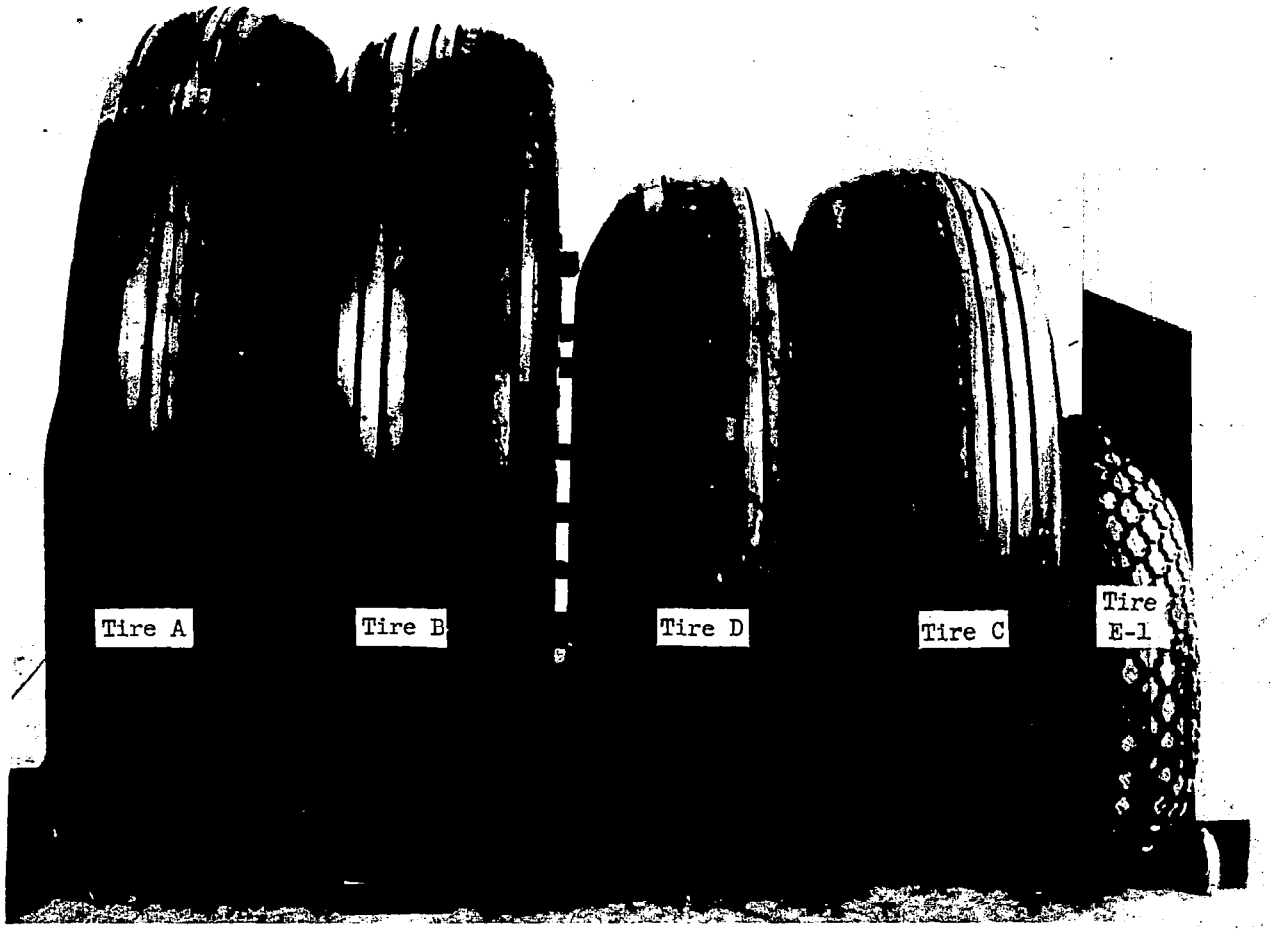


| | |
|---|---|
| Tire A | 56-inch (56 × 16), type VII (extra-high-pressure), 32-ply-rating |
| Tire B | 56-inch (56 × 16), type VII (extra-high-pressure), 24-ply-rating |
| Tire C | 45-inch (15.50-20), type III (low-pressure), 14-ply-rating |
| Tire D | 44-inch, type I (smooth-contour), 10-ply-rating |
| Tire E-1 | 27-inch, type I (smooth-contour), 10-ply-rating |

NACA
L-74867.1

Fig. 16. Photographs of test tires from NACA TN 2926.

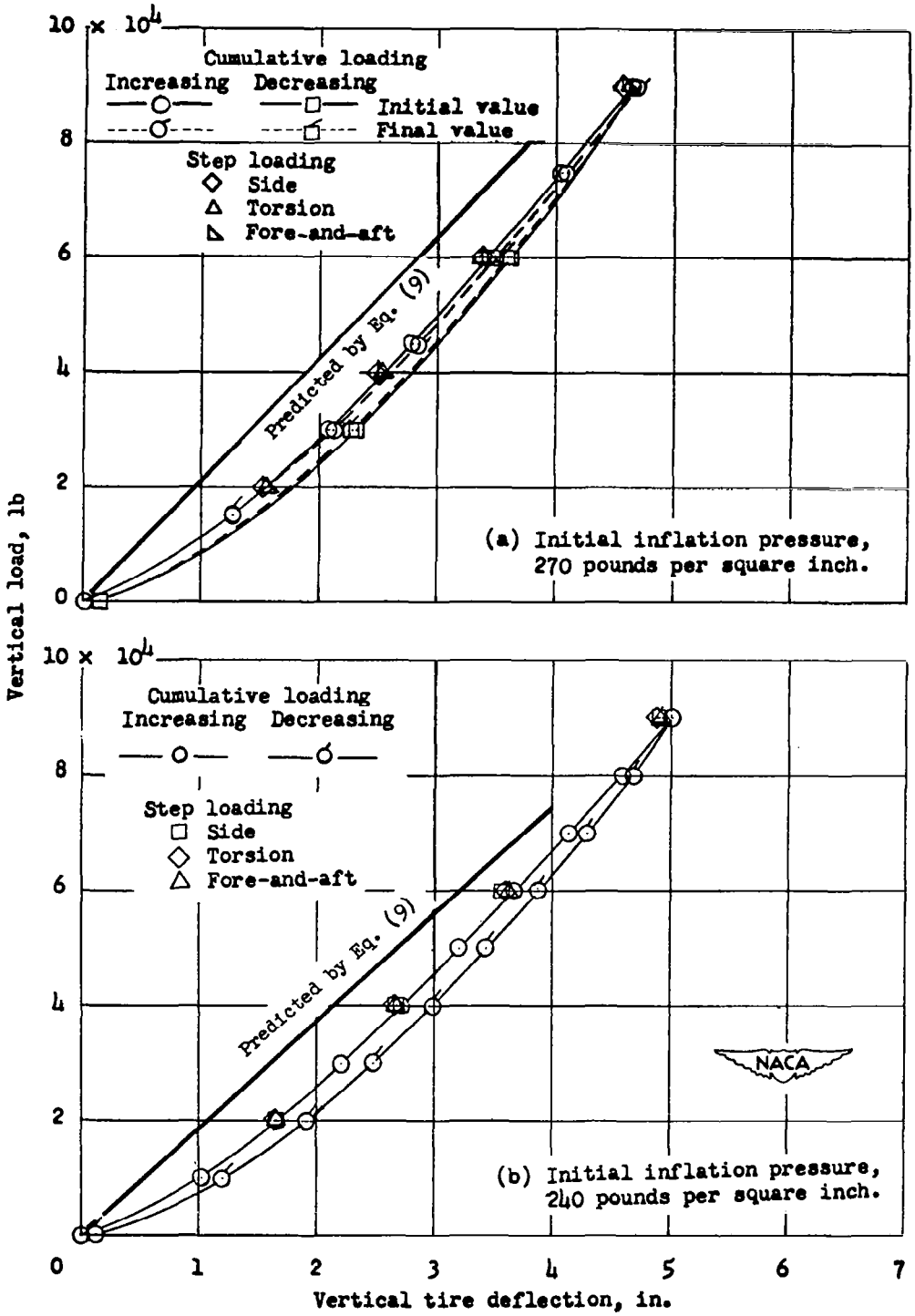


Fig. 17. Vertical load-deflection experiments vs. predictions of Eq. (9) for tire A.

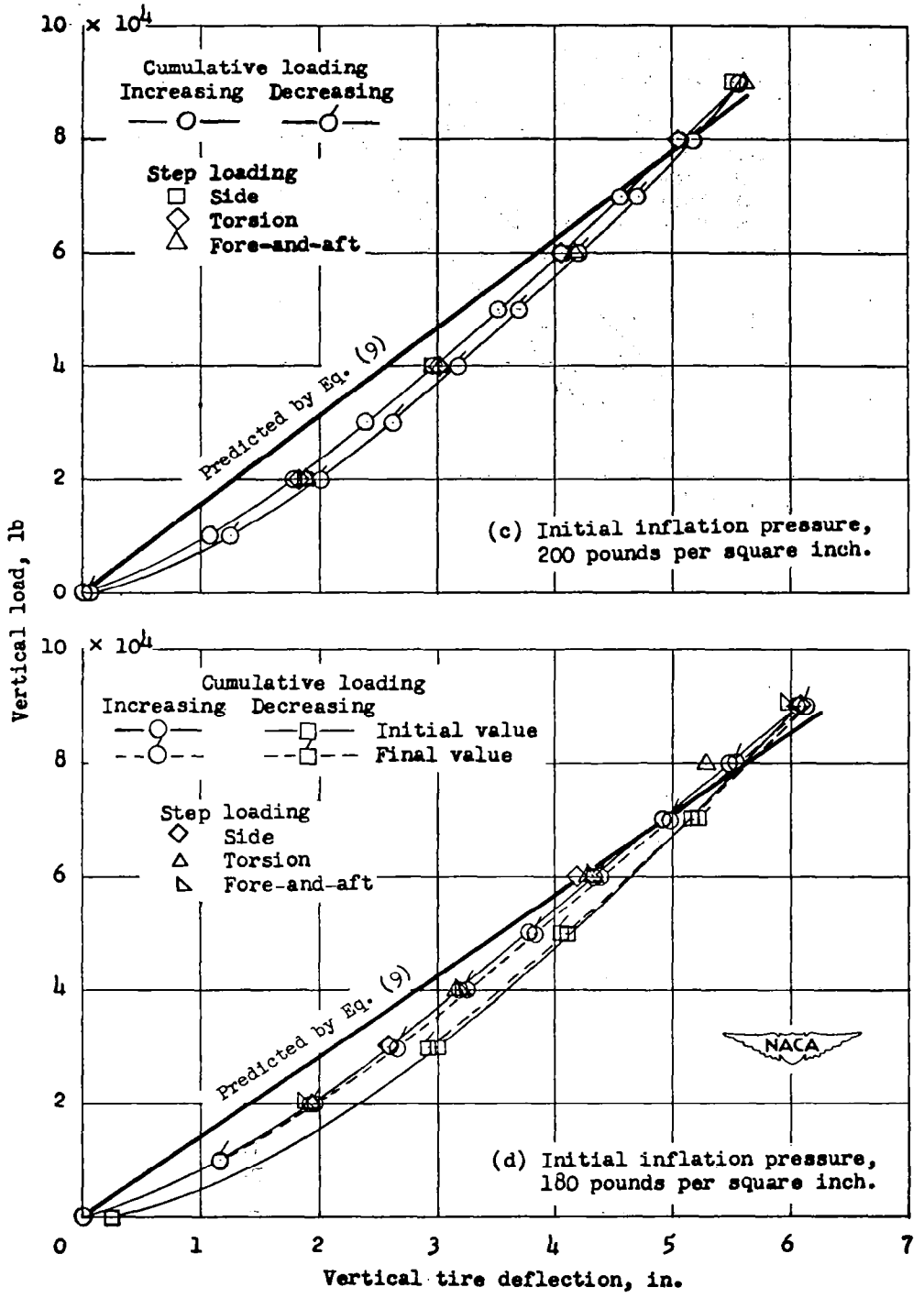


Fig. 17 (Concluded)

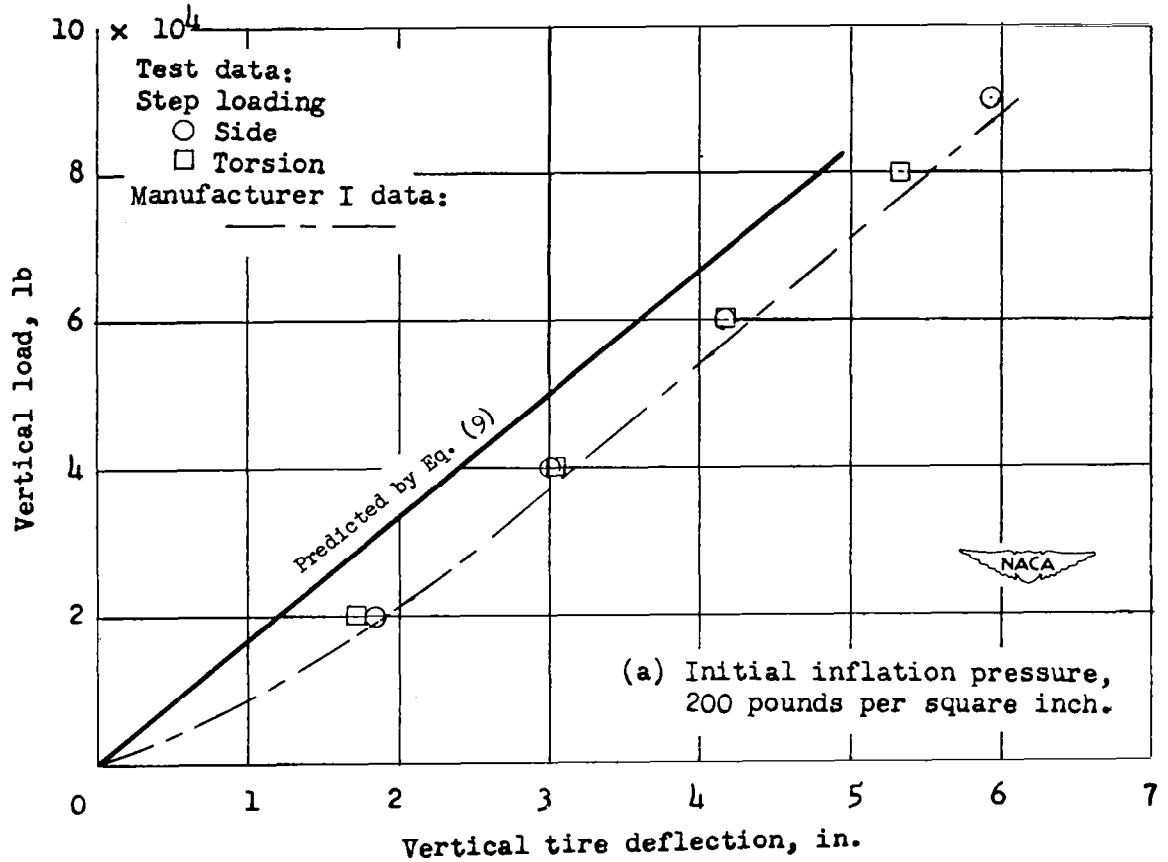


Fig. 18. Vertical load-deflection experiments vs. predictions of Eq. (9) for tire B.

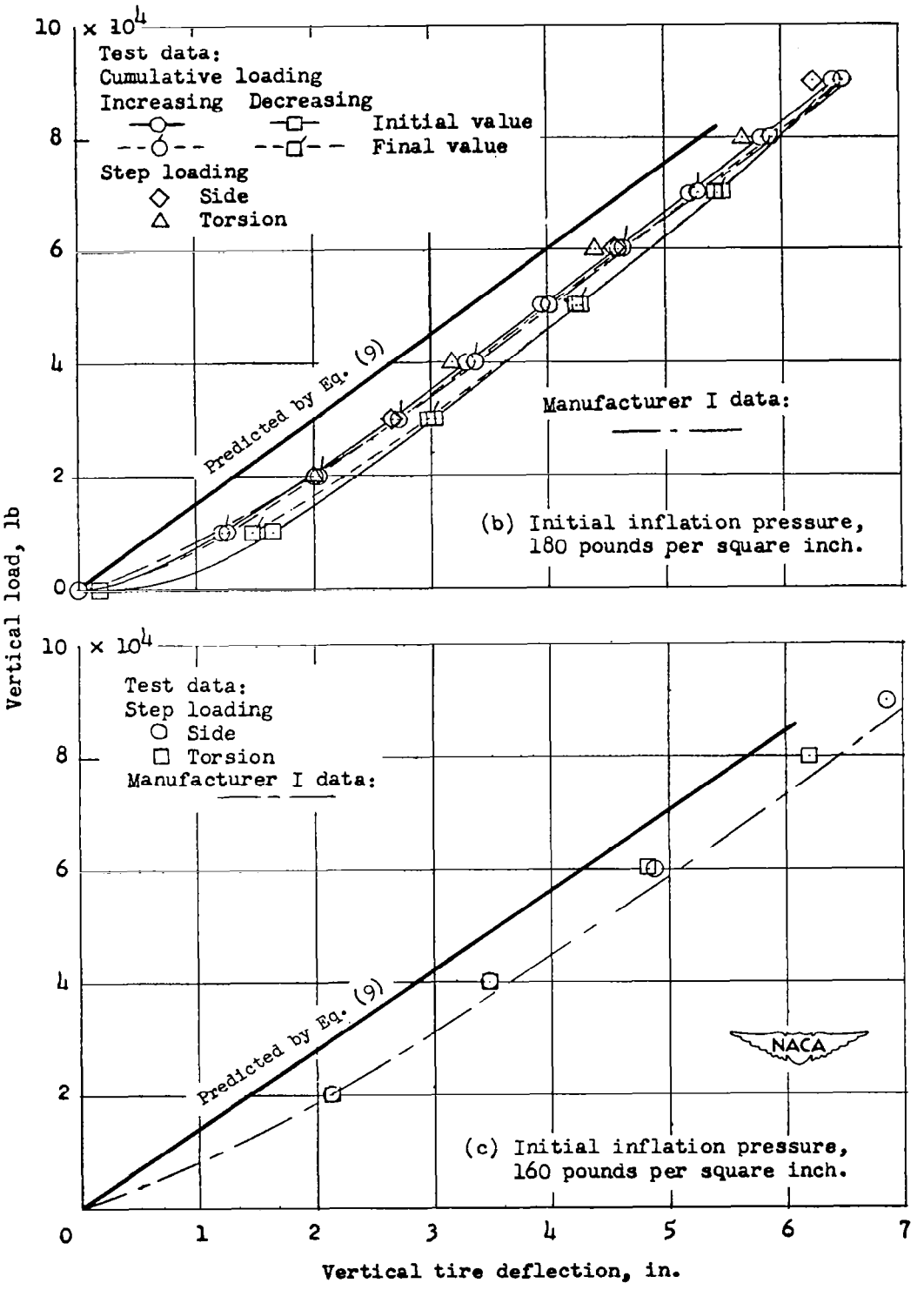


Fig. 18 (Concluded)

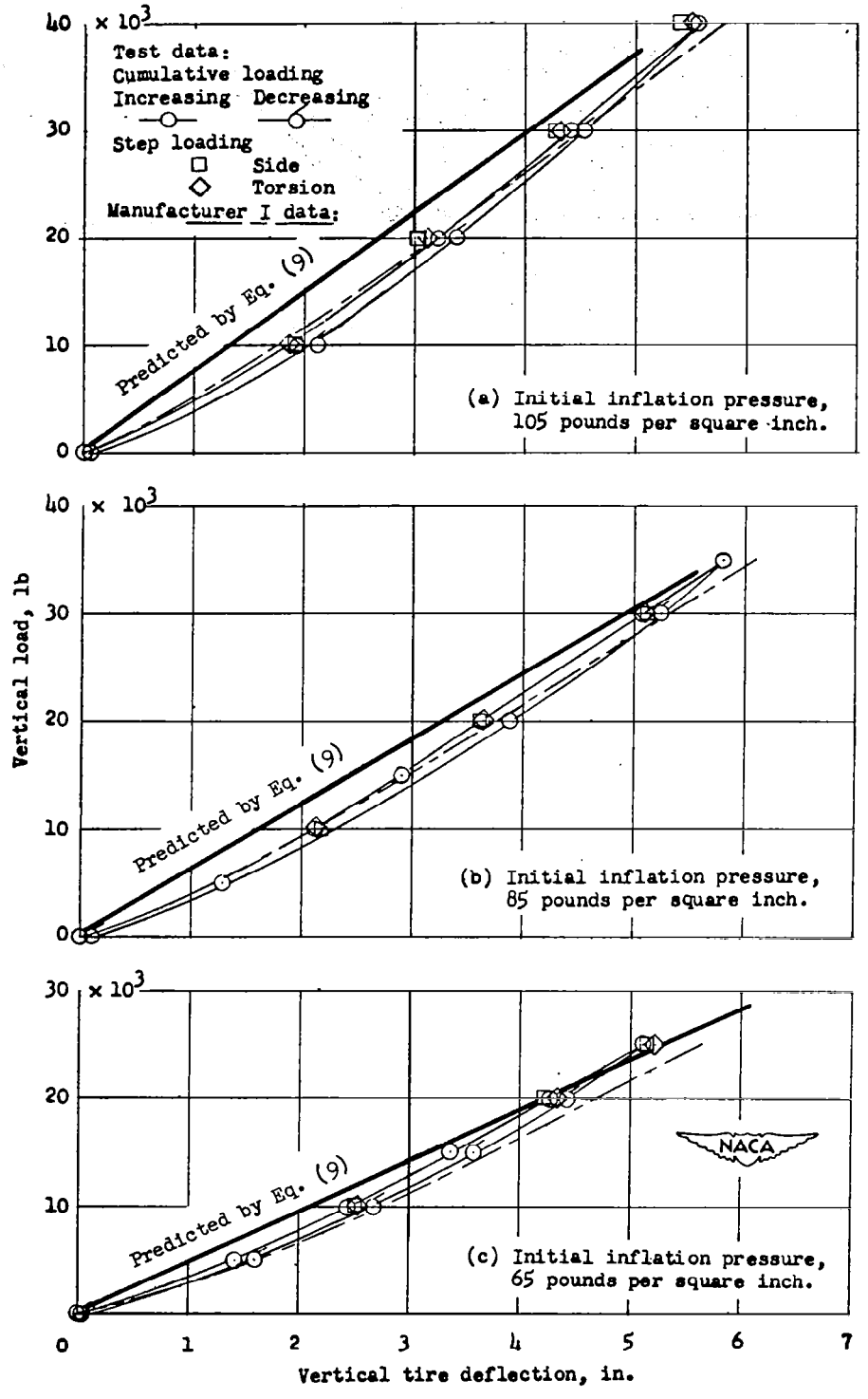


Fig. 19. Vertical load-deflection experiments vs. predictions of Eq. (9) for tire C.

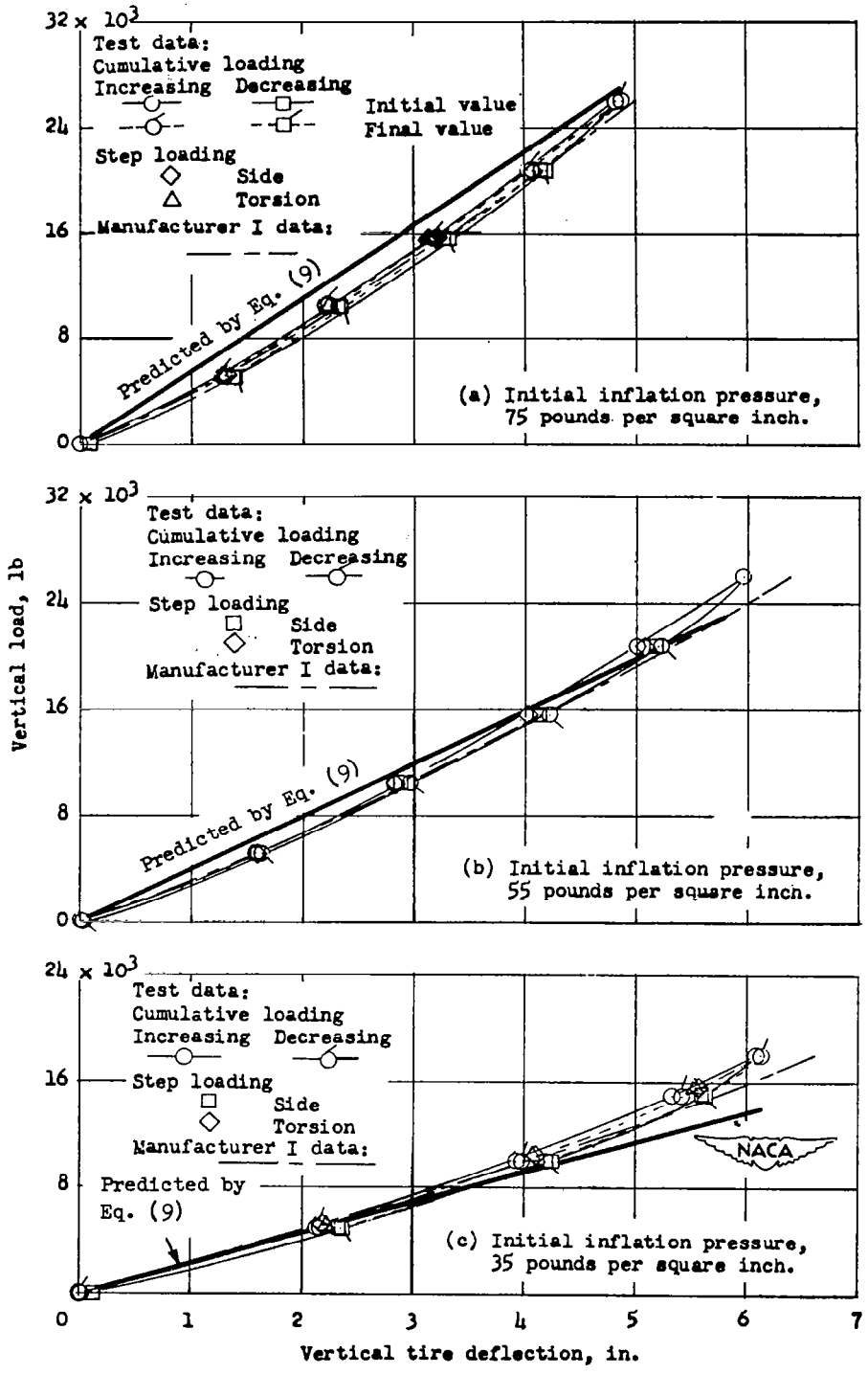


Fig. 20. Vertical load-deflection experiments vs. predictions of Eq. (9) for tire D.

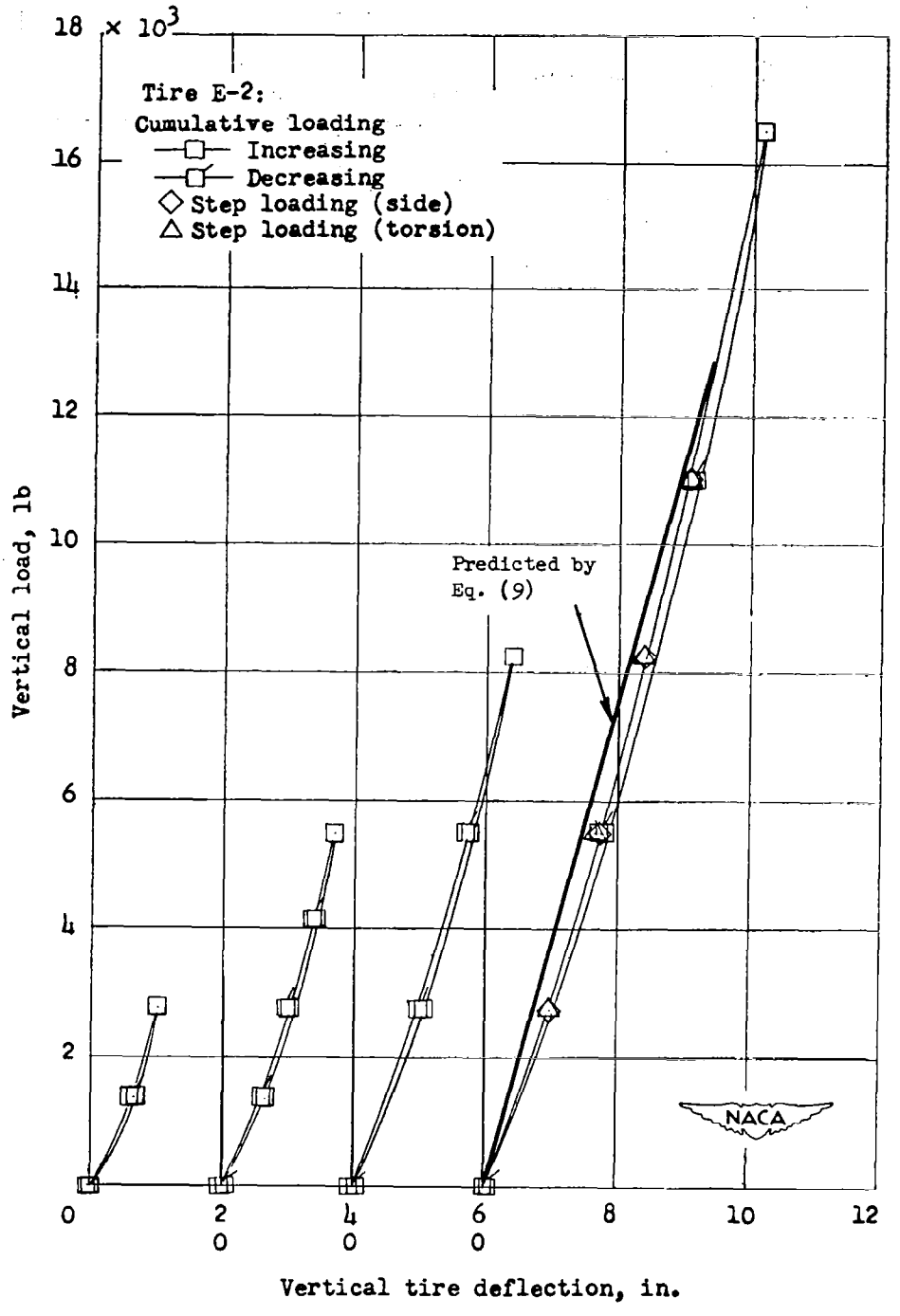


(a) Initial inflation pressure, 80 pounds per square inch; tire E-2.

Fig. 21. Vertical load-deflection experiments vs. predictions of Eq. (9) for tire E.

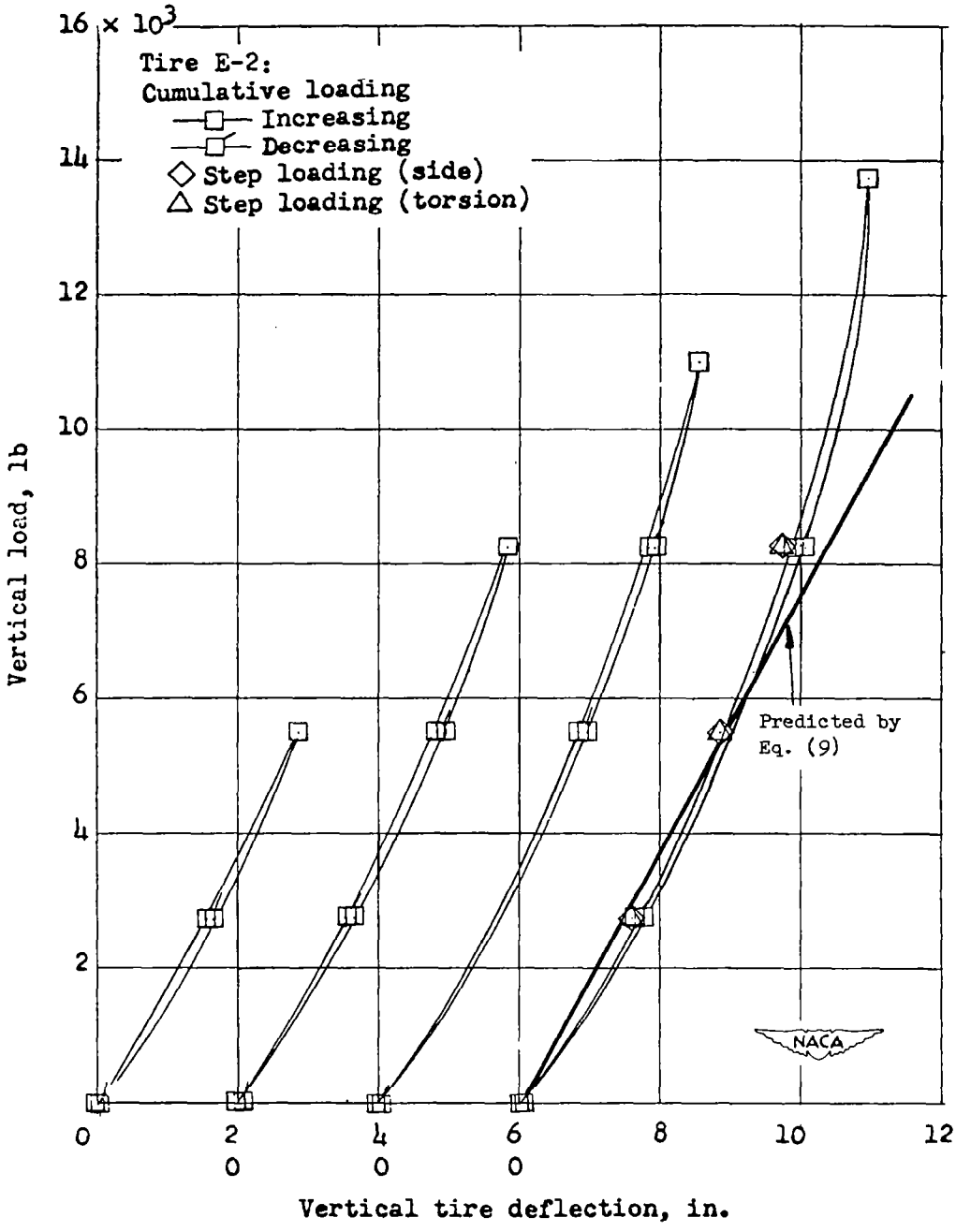


(b) Initial inflation pressure, 40 pounds per square inch; tire E-2.

Fig. 21 (Continued)

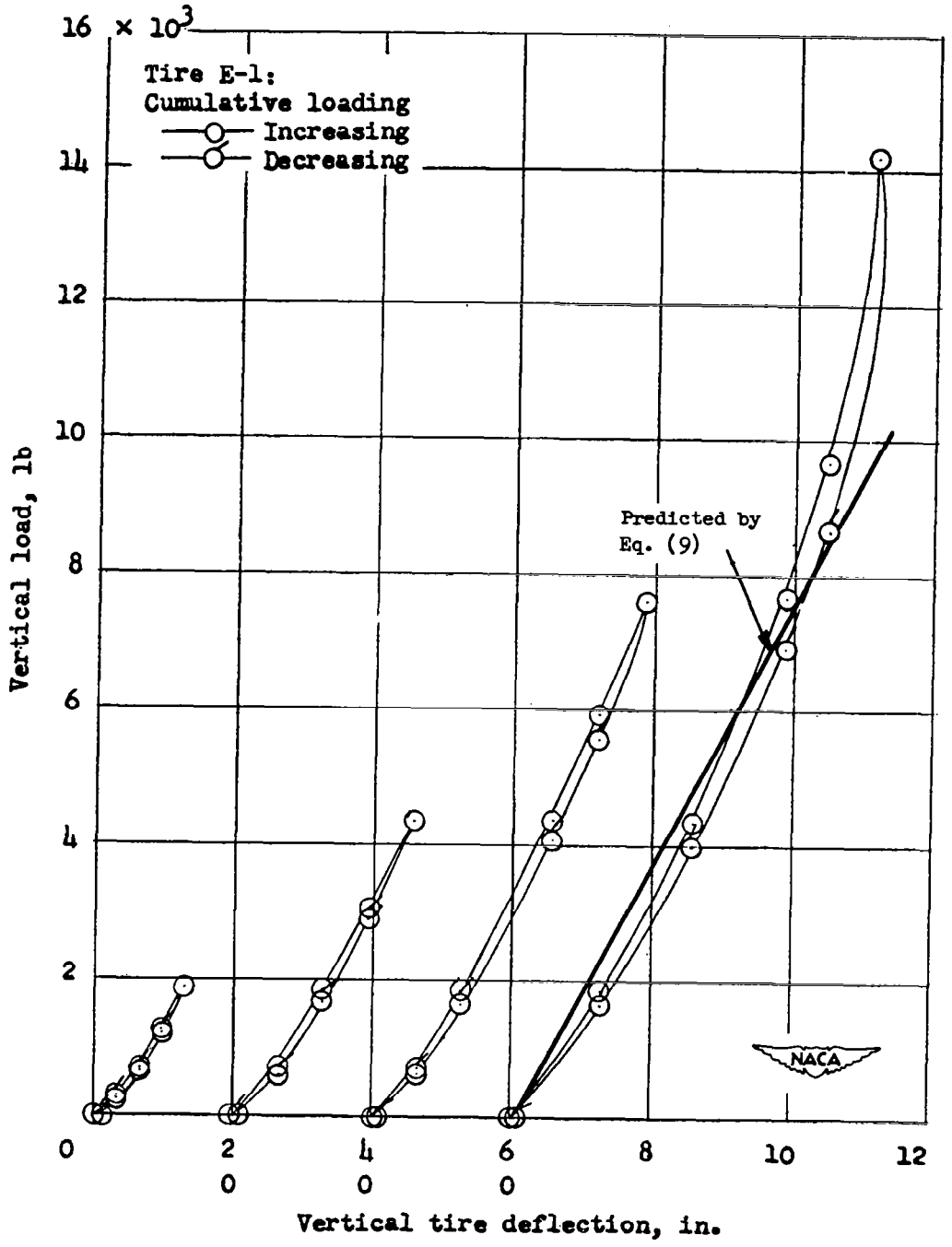


(c) Initial inflation pressure, 40 pounds per square inch; tire E-1.

Fig. 21 (Continued)

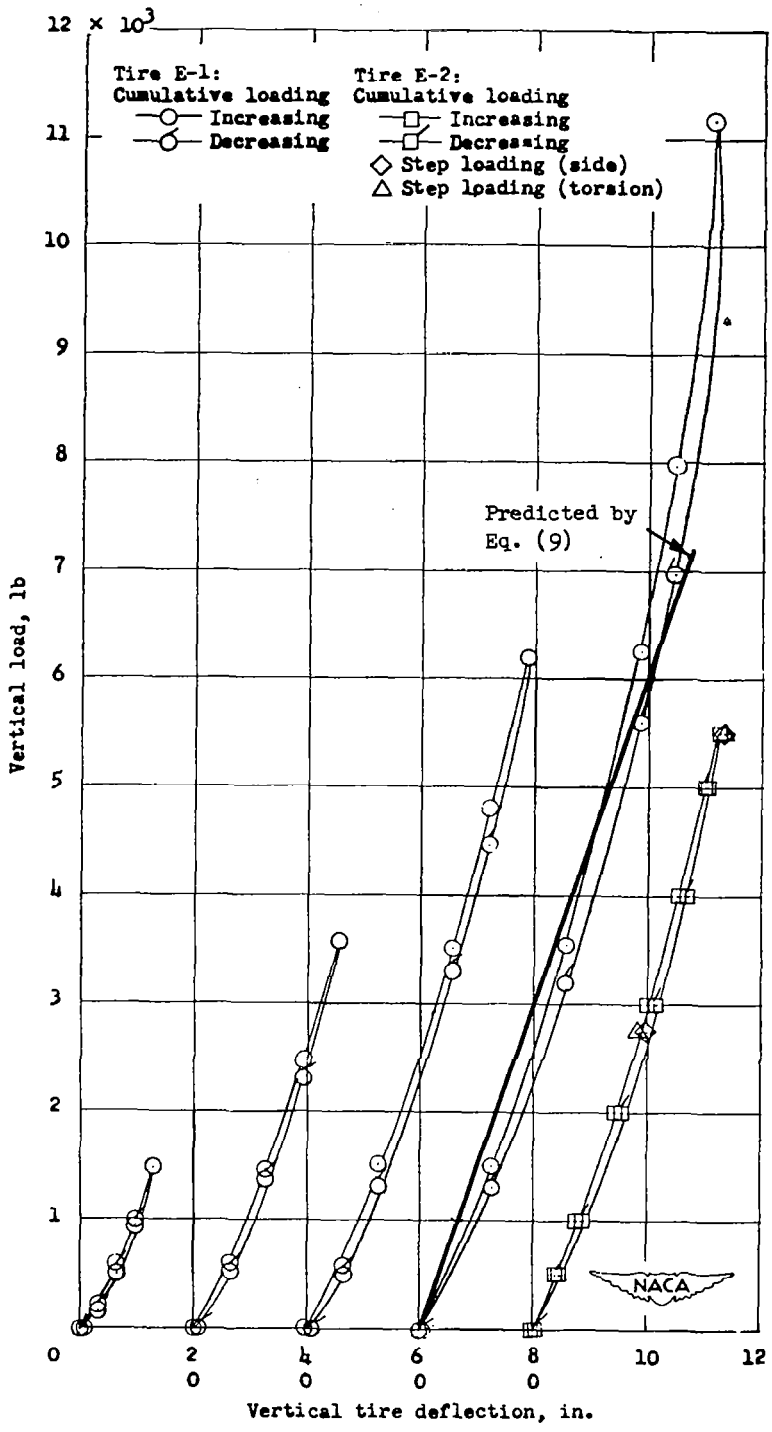


(d) Initial inflation pressure, 32 pounds per square inch; tires E-1 and E-2.

Fig. 21 (Continued)

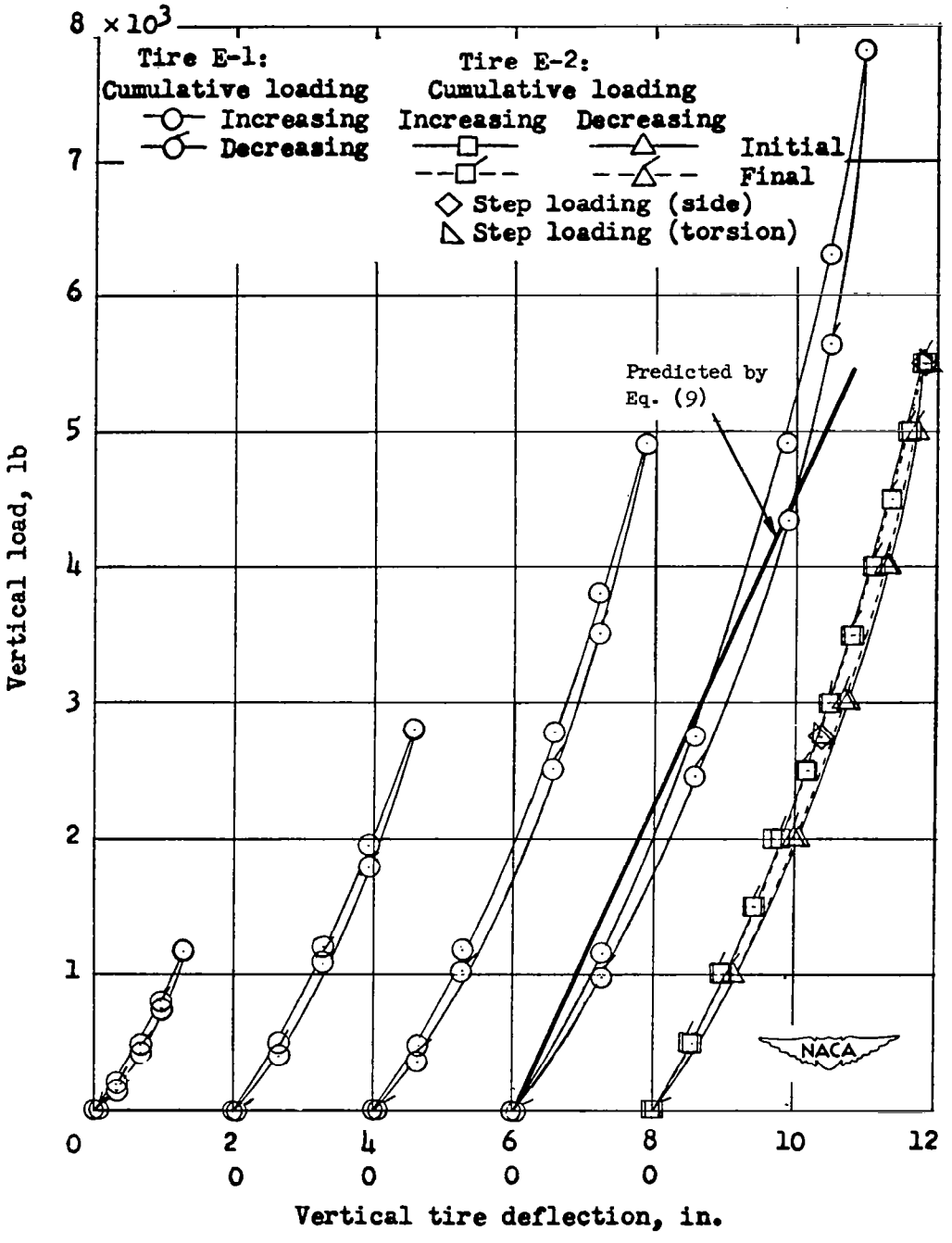


(e) Initial inflation pressure, 24 pounds per square inch; tires E-1 and E-2.

Fig. 21 (Concluded)

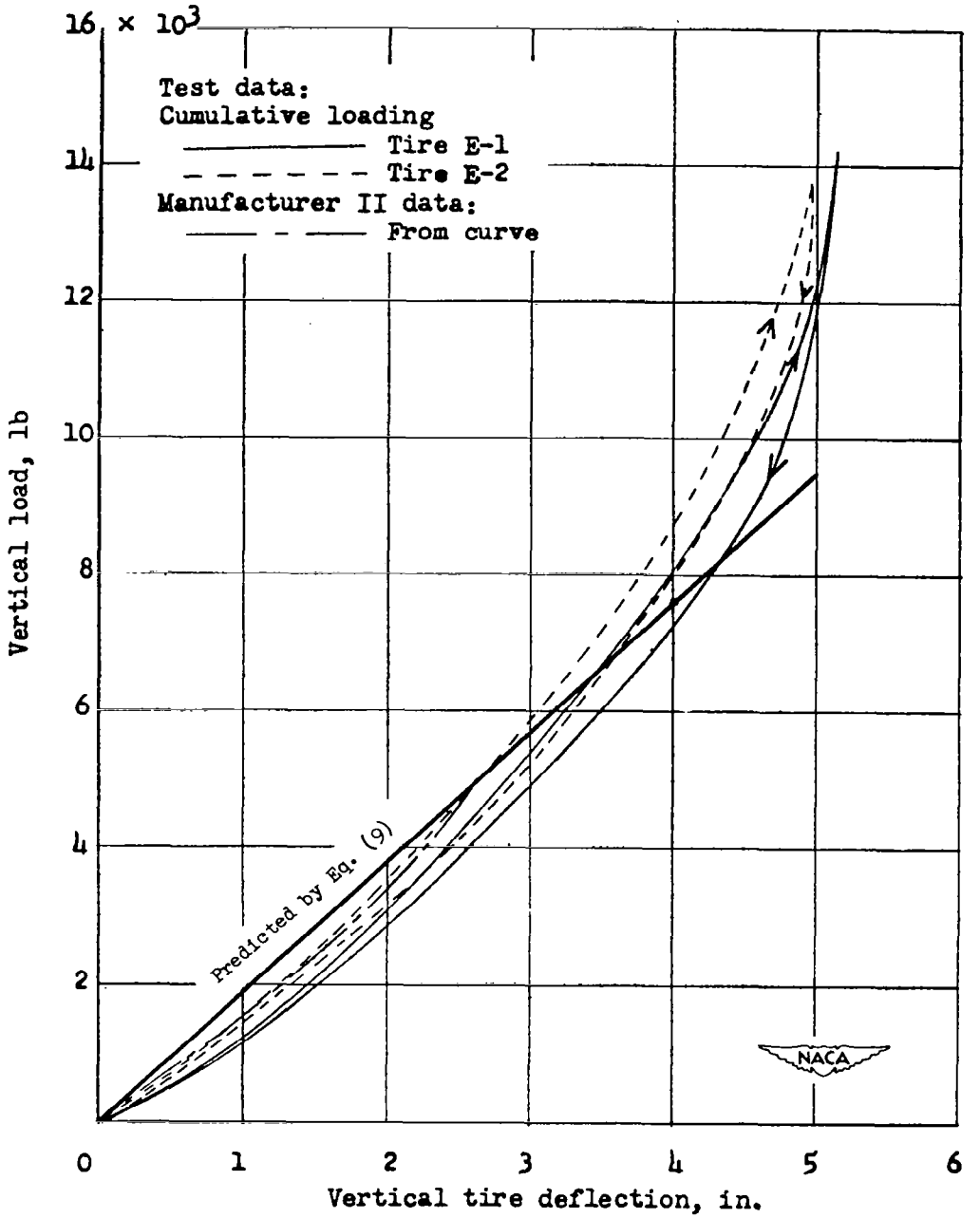


(a) Initial inflation pressure, 40 pounds per square inch.

Fig. 22. Vertical load-deflection experiments vs. predictions of Eq. (9) for two types of tire E.

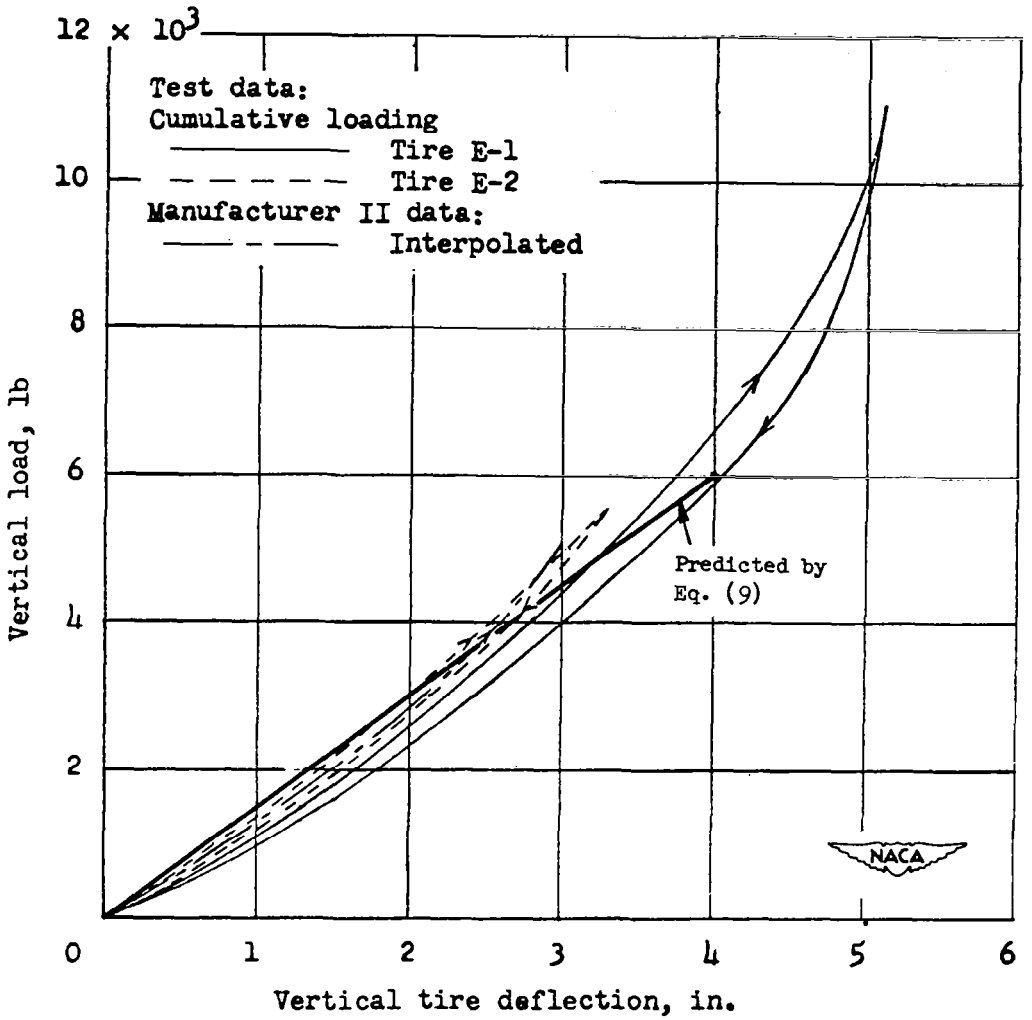


(b) Initial inflation pressure, 32 pounds per square inch.

Fig. 22 (Continued)

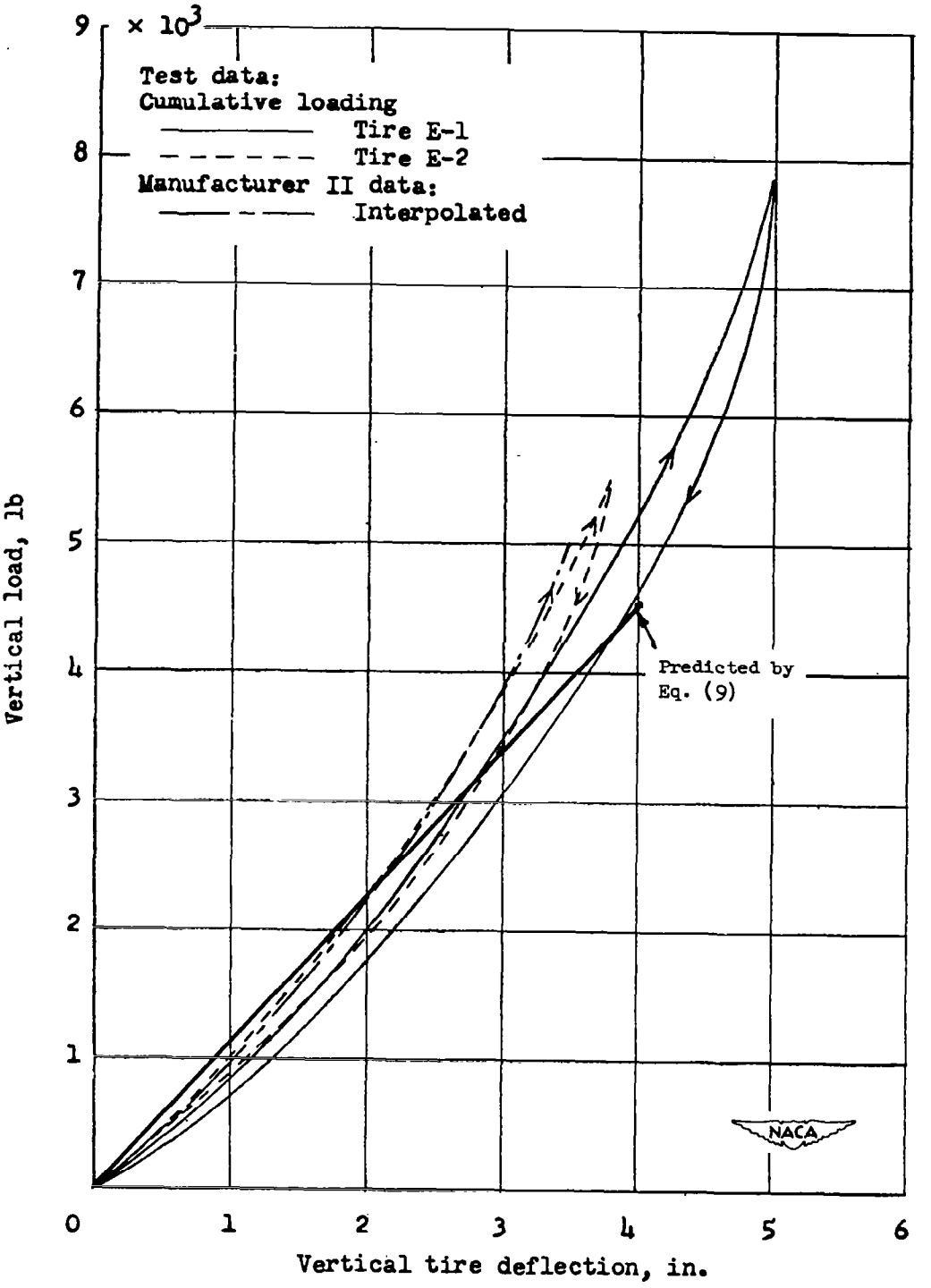


(c) Initial inflation pressure, 24 pounds per square inch.

Fig. 22 (Concluded)

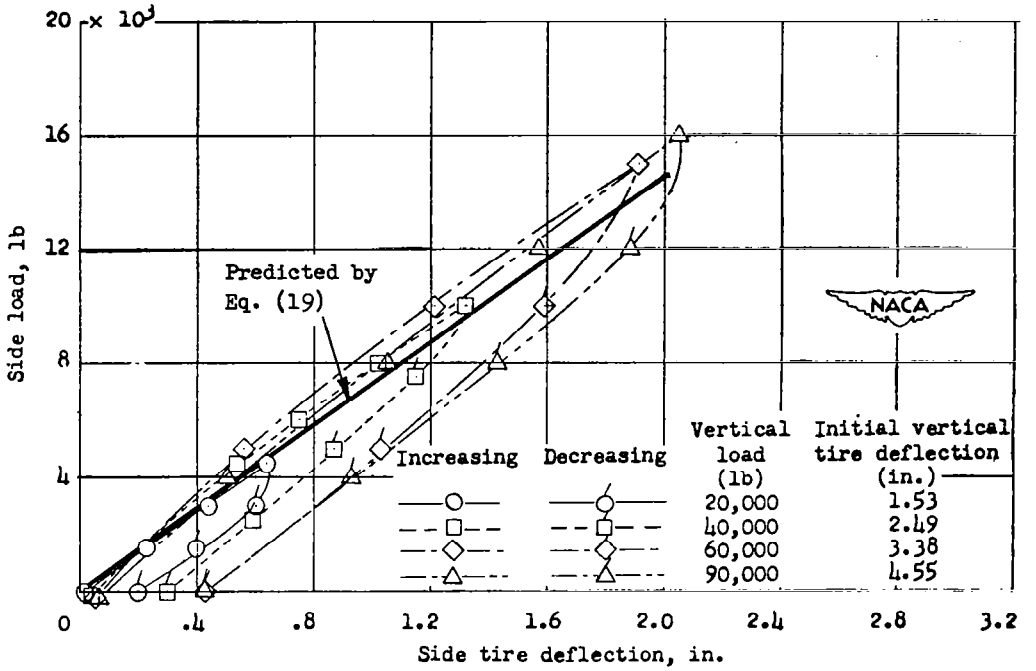


(a) Initial inflation pressure, 270 pounds per square inch.

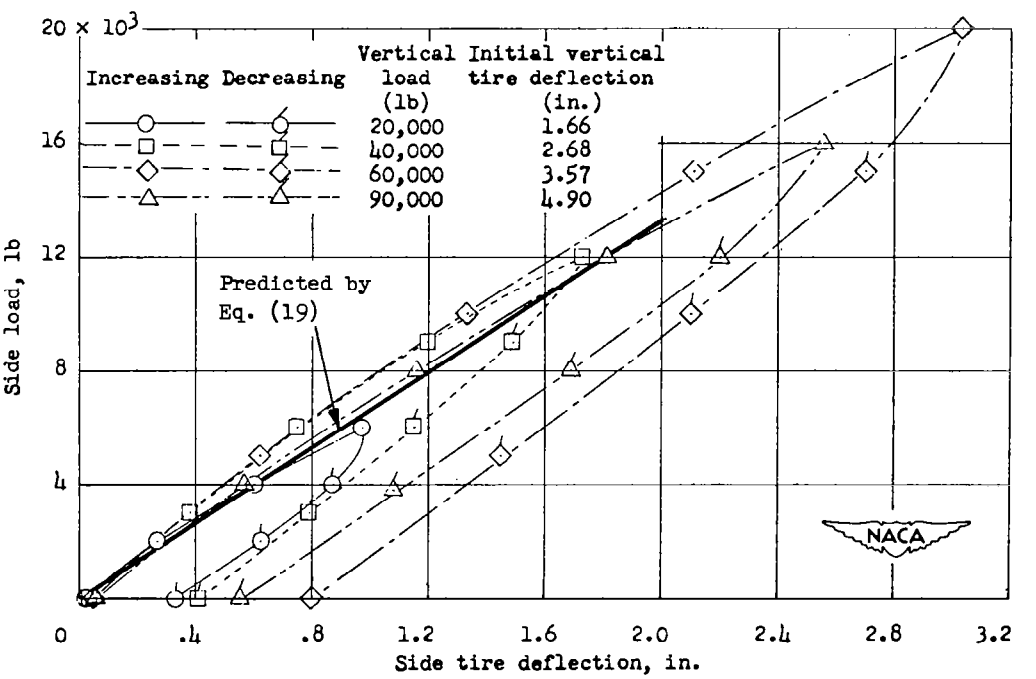


(b) Initial inflation pressure, 240 pounds per square inch.

Fig. 23. Side load-deflection experiments vs. predictions of Eq. (19) for tire A.

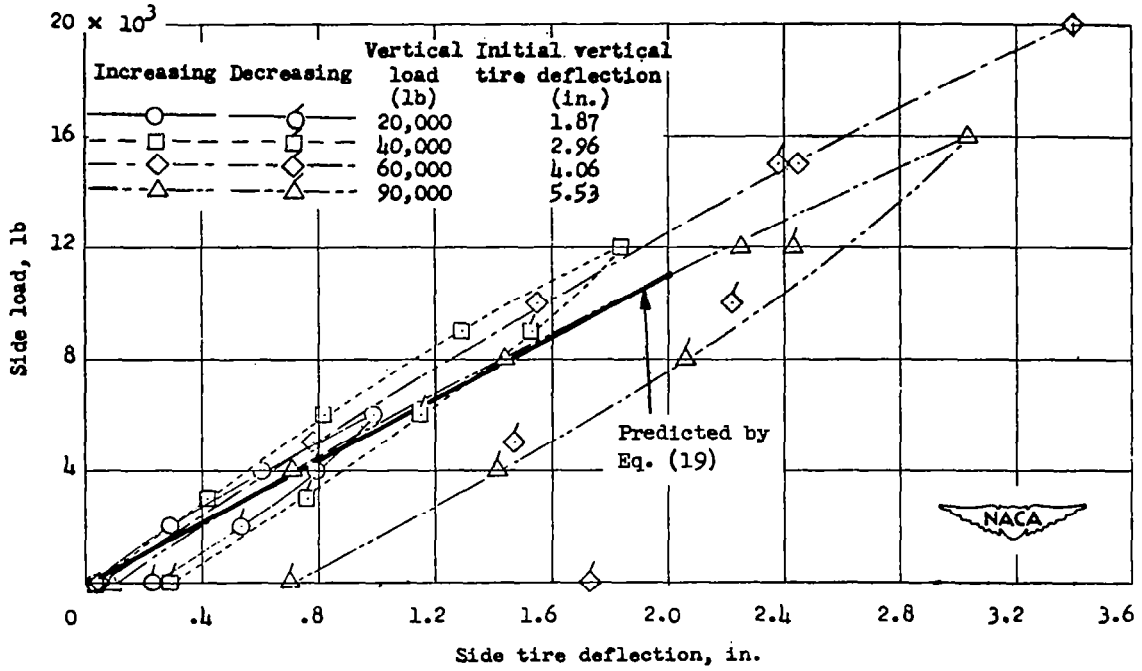


(c) Initial inflation pressure, 200 pounds per square inch.

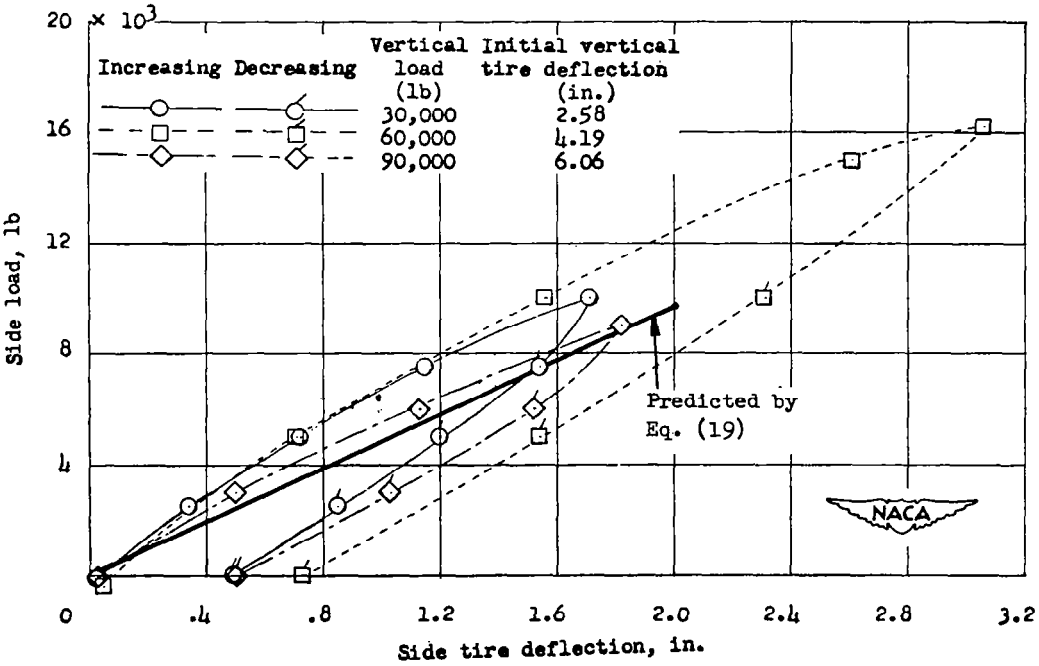


(d) Initial inflation pressure, 180 pounds per square inch.

Fig. 23 (Concluded)

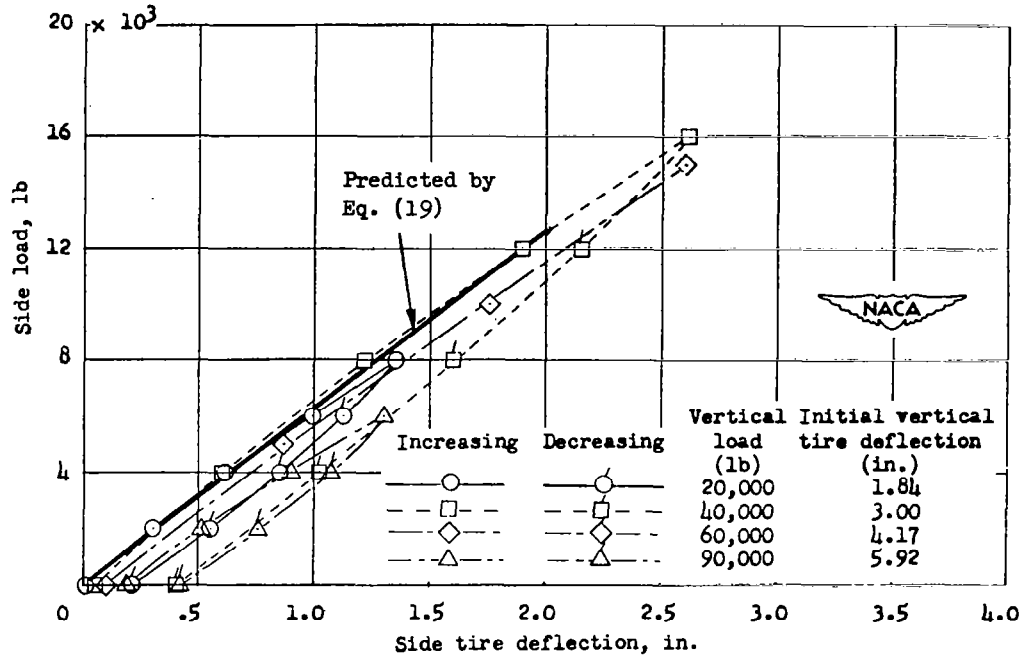


(a) Initial inflation pressure, 200 pounds per square inch.

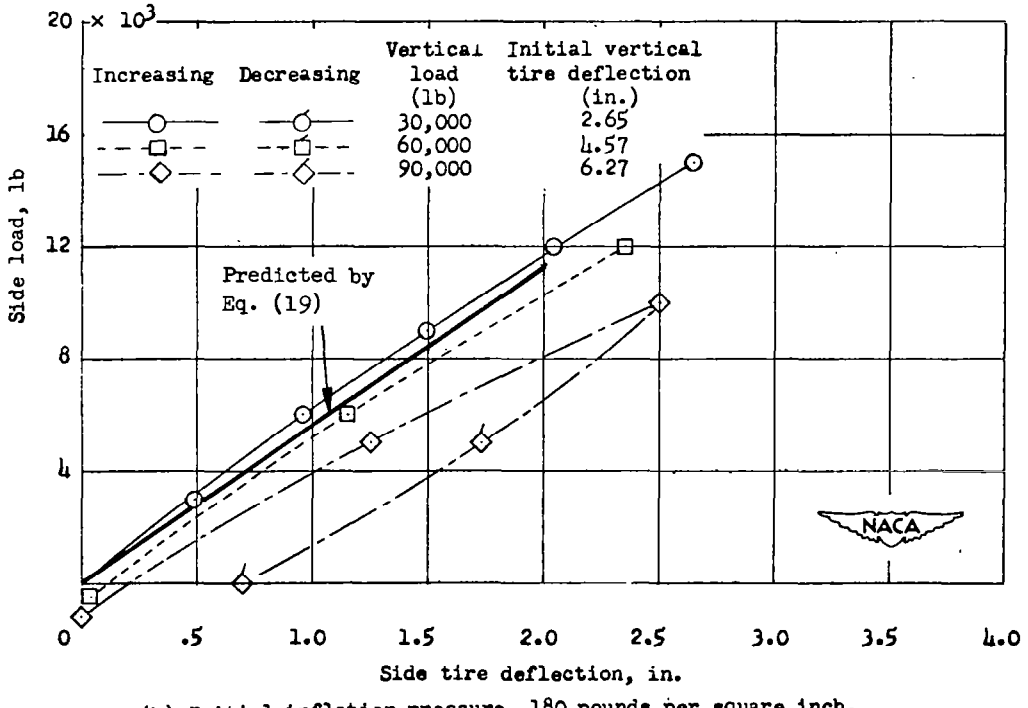


(b) Initial inflation pressure, 180 pounds per square inch.

Fig. 24. Side load-deflection experiments vs. predictions of Eq. (19) for tire B.

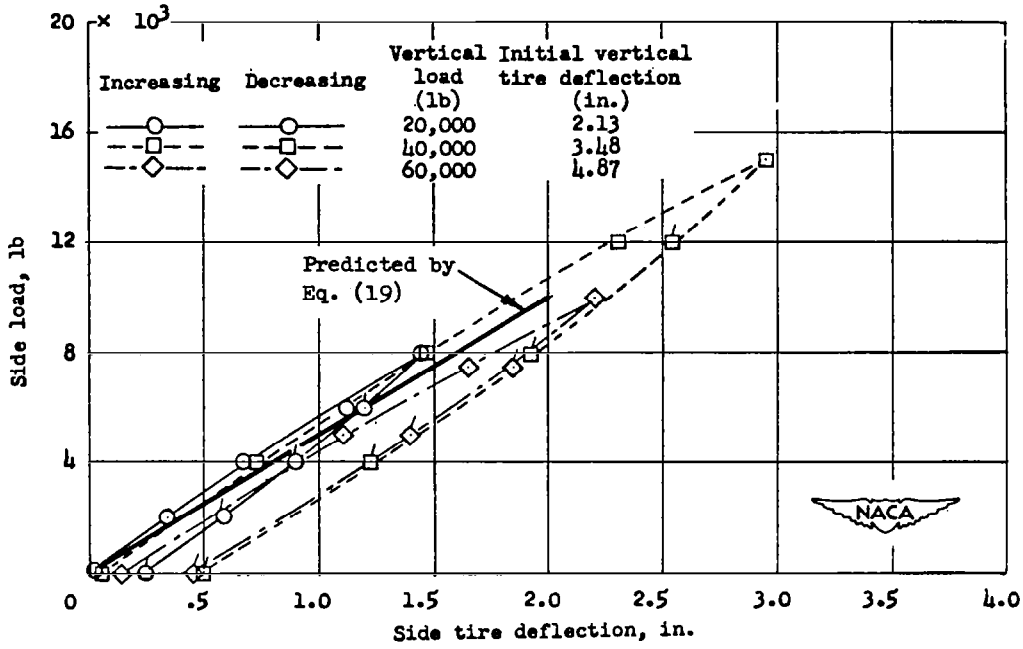


(c) Initial inflation pressure, 160 pounds per square inch.

Fig. 24 (Concluded)

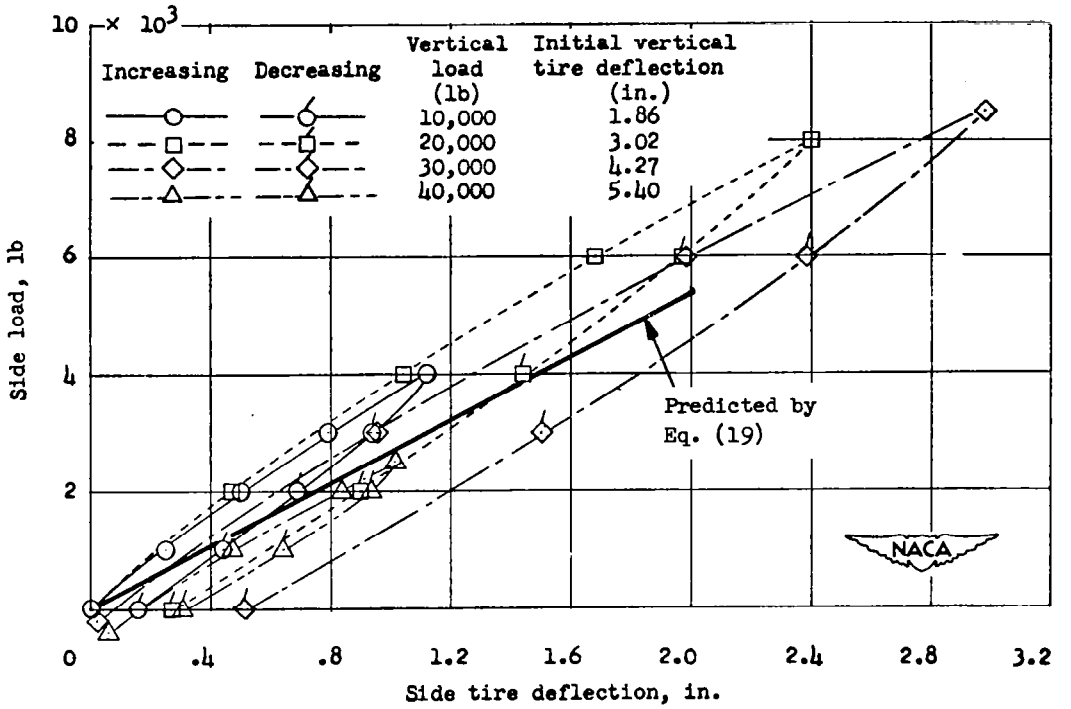


(a) Initial inflation pressure, 105 pounds per square inch.

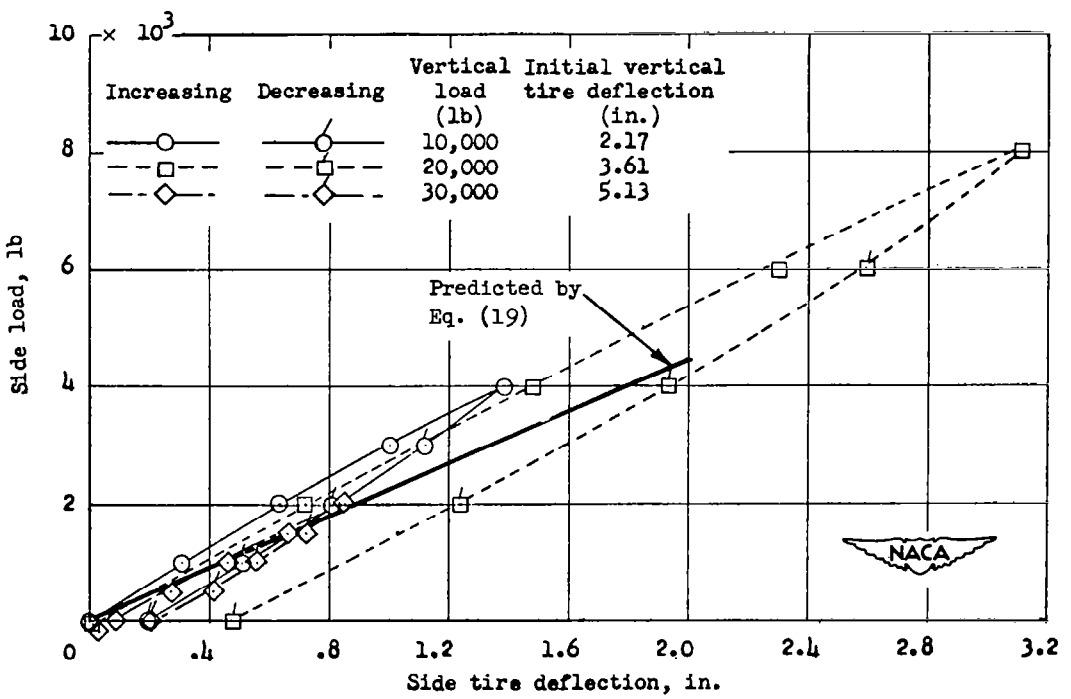


(b) Initial inflation pressure, 85 pounds per square inch.

Fig. 25. Side load-deflection experiments vs. predictions of Eq. (19) for tire C.

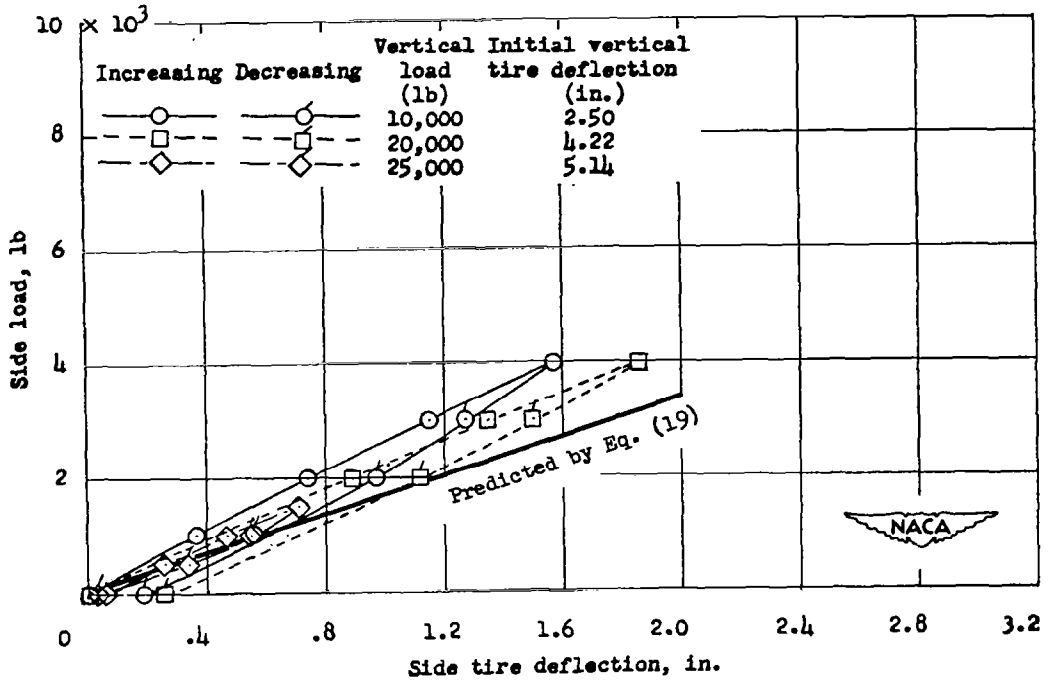


(c) Initial inflation pressure, 65 pound per square inch.

Fig. 25 (Concluded)

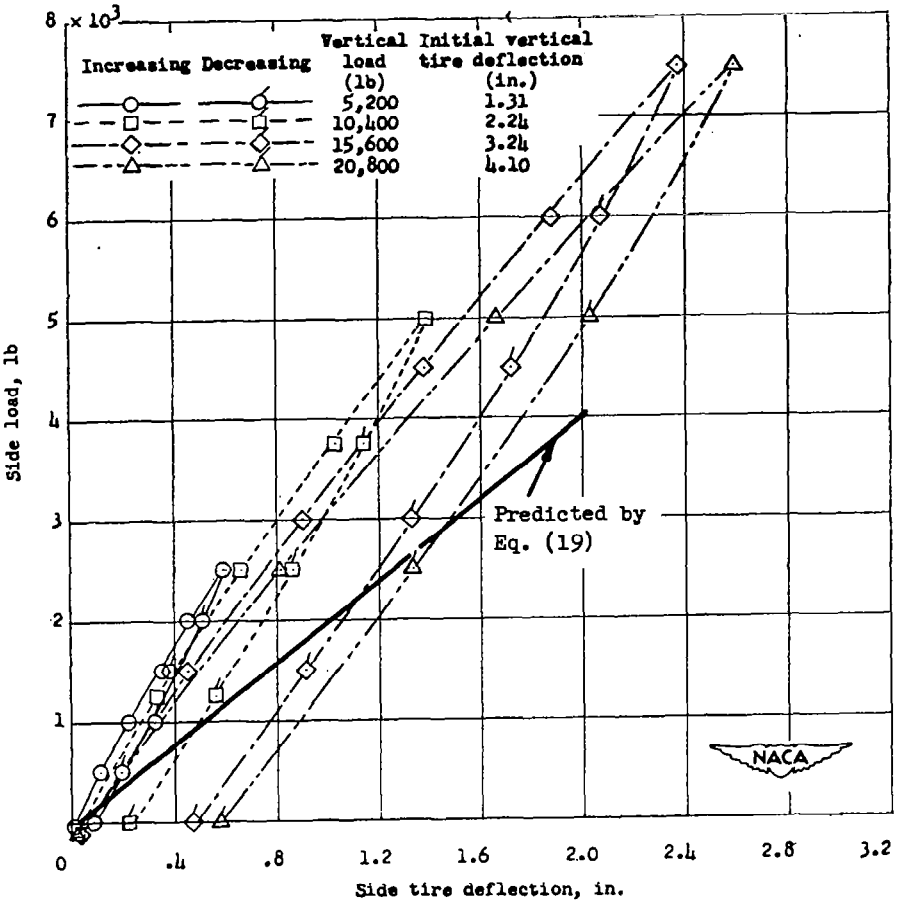


(a) Initial inflation pressure, 75 pounds per square inch.

Fig. 26. Side load-deflection experiments vs. predictions of Eq. (19) for tire D.

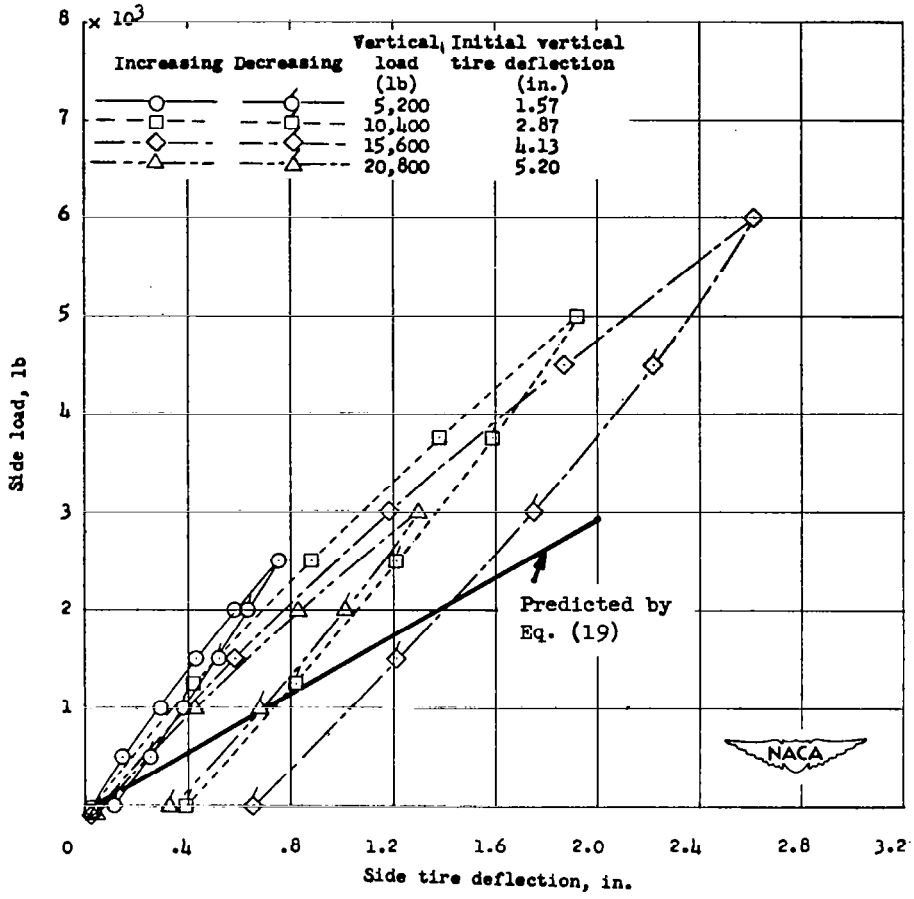


(b) Initial inflation pressure, 55 pounds per square inch.

Fig. 26 (Continued)

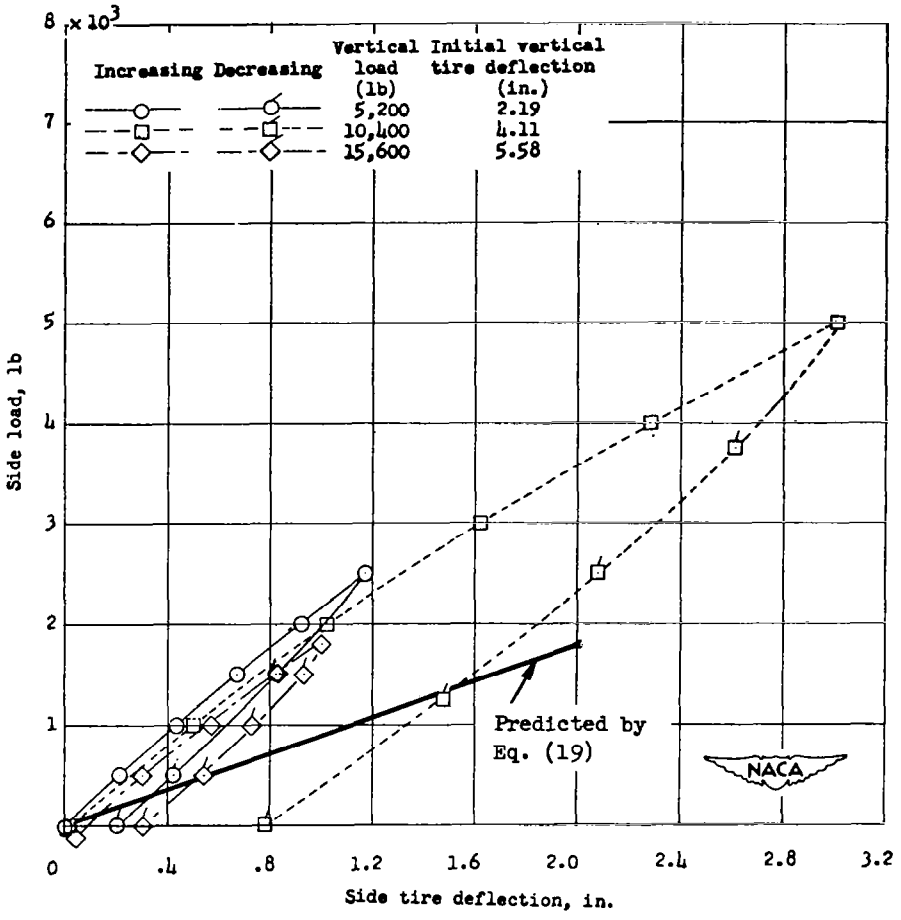


(c) Initial inflation pressure, 35 pounds per square inch.

Fig. 26 (Concluded)

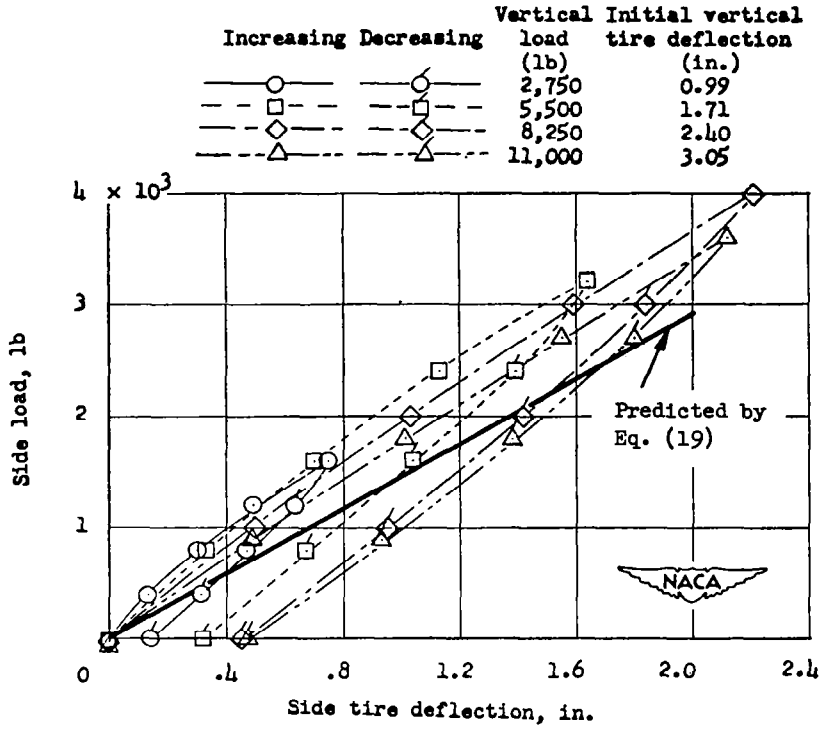


(a) Initial inflation pressure, 80 pounds per square inch.

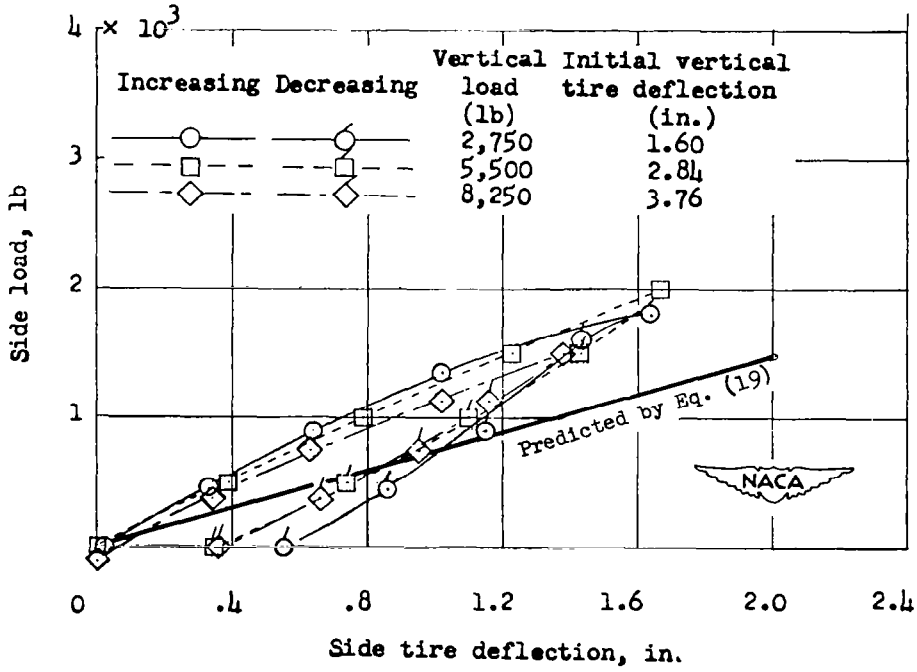


(b) Initial inflation pressure, 40 pounds per square inch.

Fig. 27. Side load-deflection experiments vs. predictions of Eq. (19) for tire E.

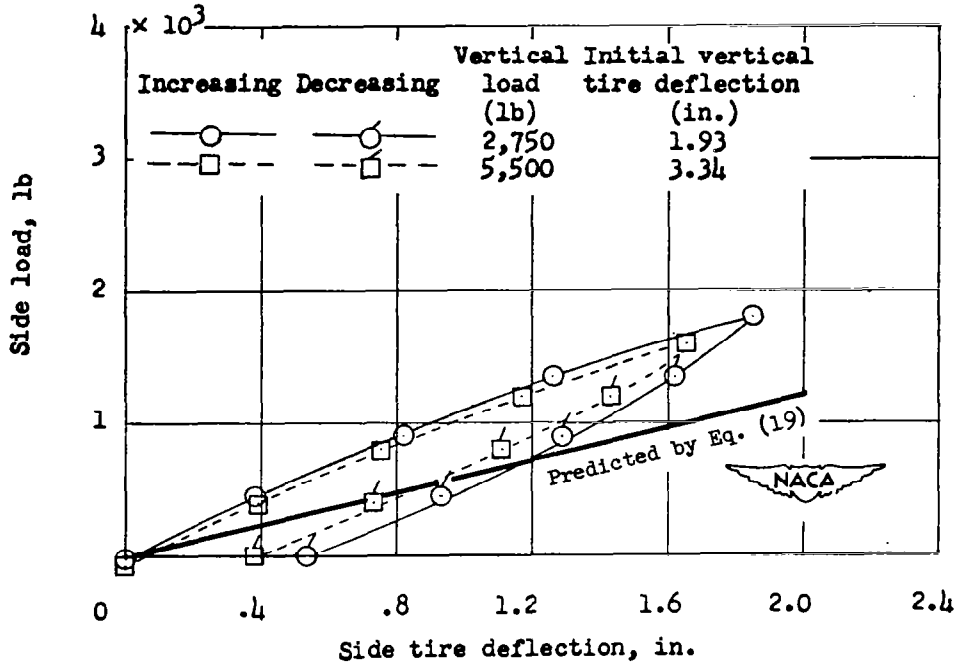


(c) Initial inflation pressure, 32 pounds per square inch.

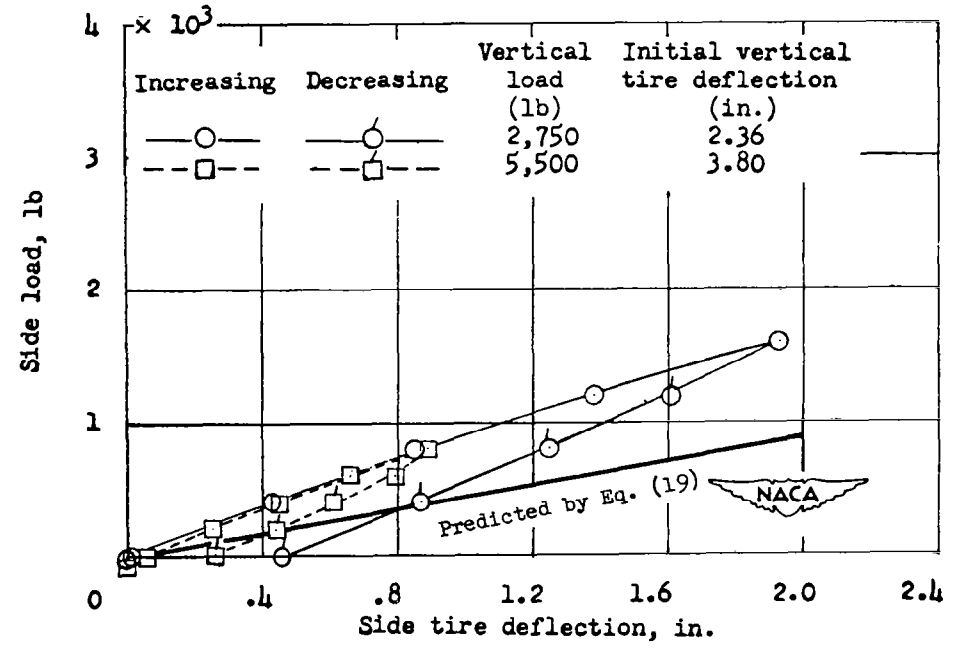


(d) Initial inflation pressure, 24 pounds per square inch.

Fig. 27 (Concluded)

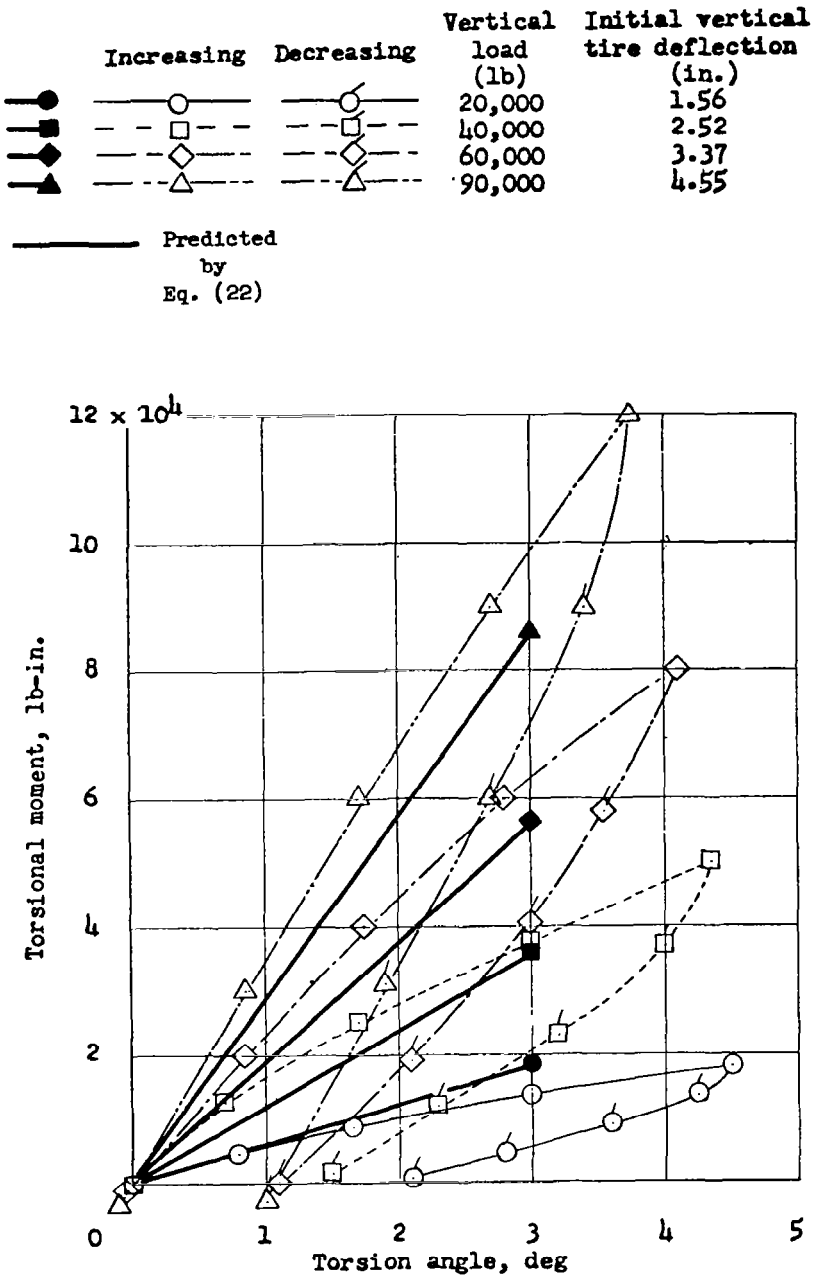


(a) Initial inflation pressure, 270 pounds per square inch.

Fig. 28. Moment-angle of twist experiments vs. predictions of Eq. (22) for tire A.

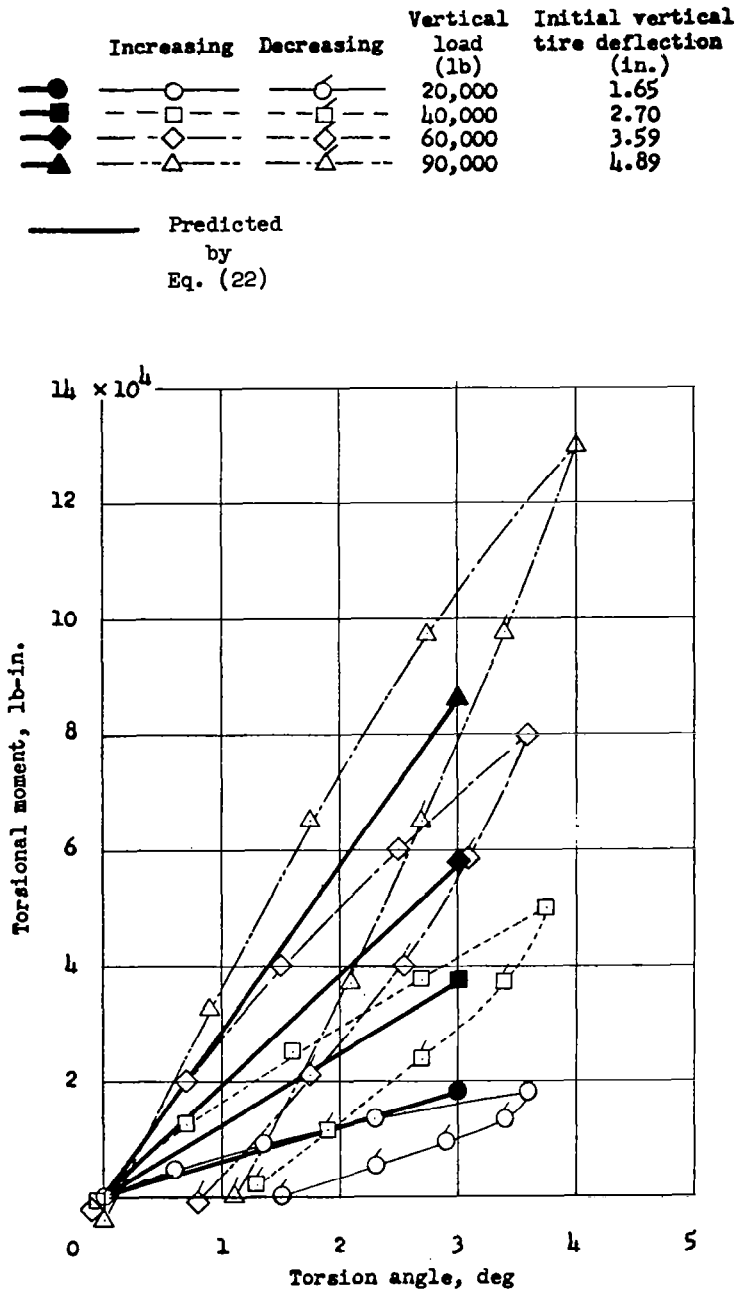


(b) Initial inflation pressure, 240 pounds per square inch.

Fig. 28 (Continued)

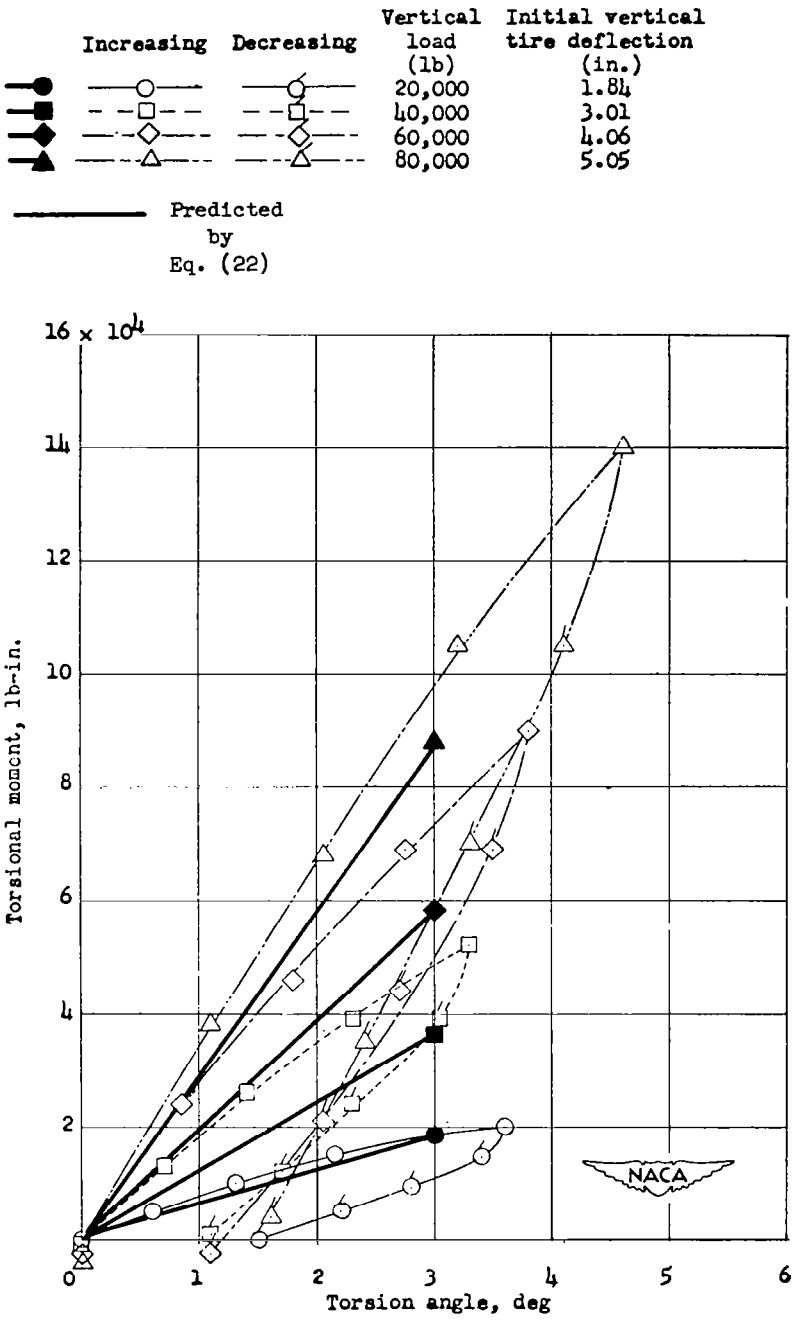


(c) Initial inflation pressure, 200 pounds per square inch.

Fig. 28 (Continued)

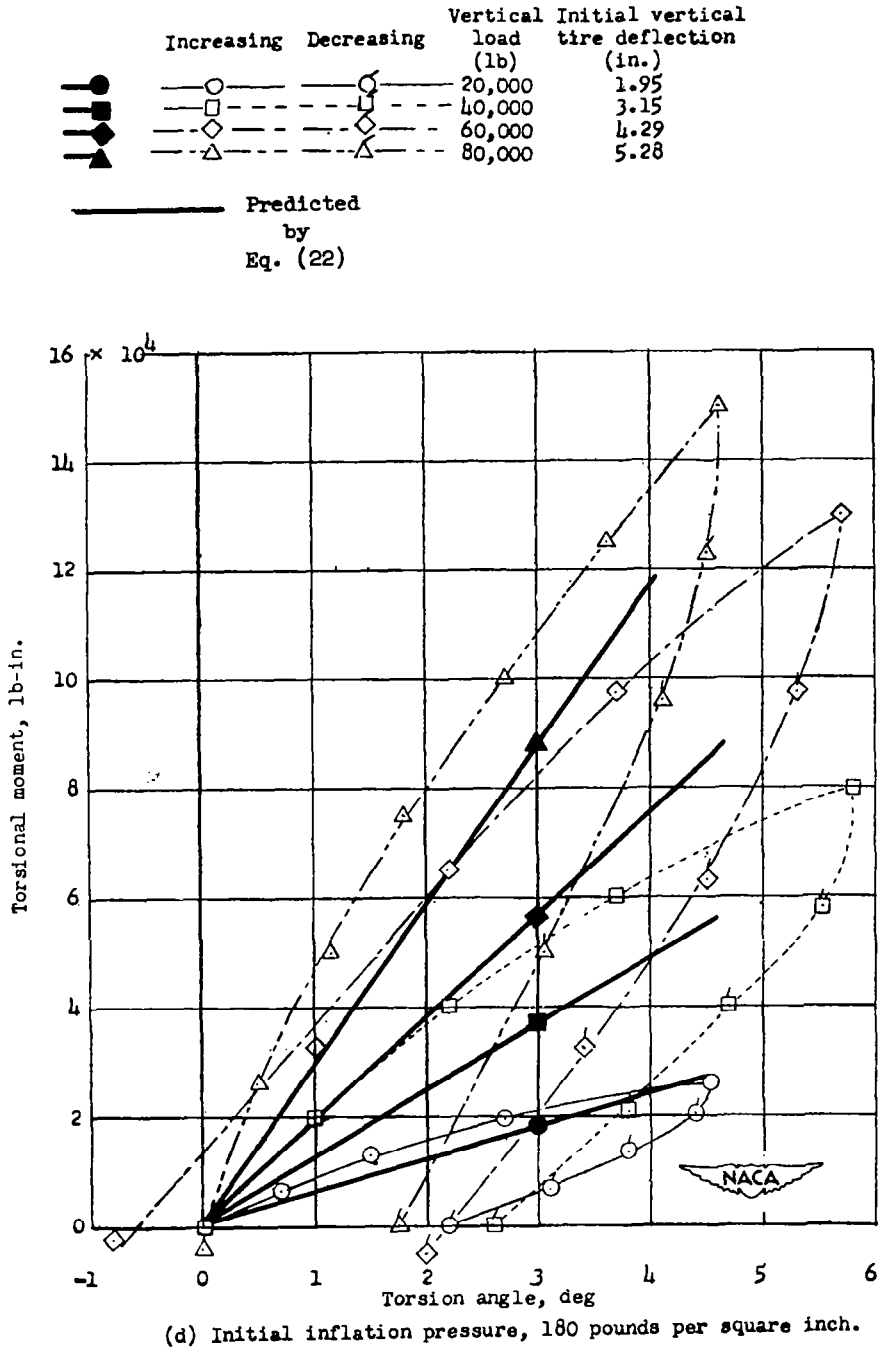


(d) Initial inflation pressure, 180 pounds per square inch.

Fig. 28 (Concluded)

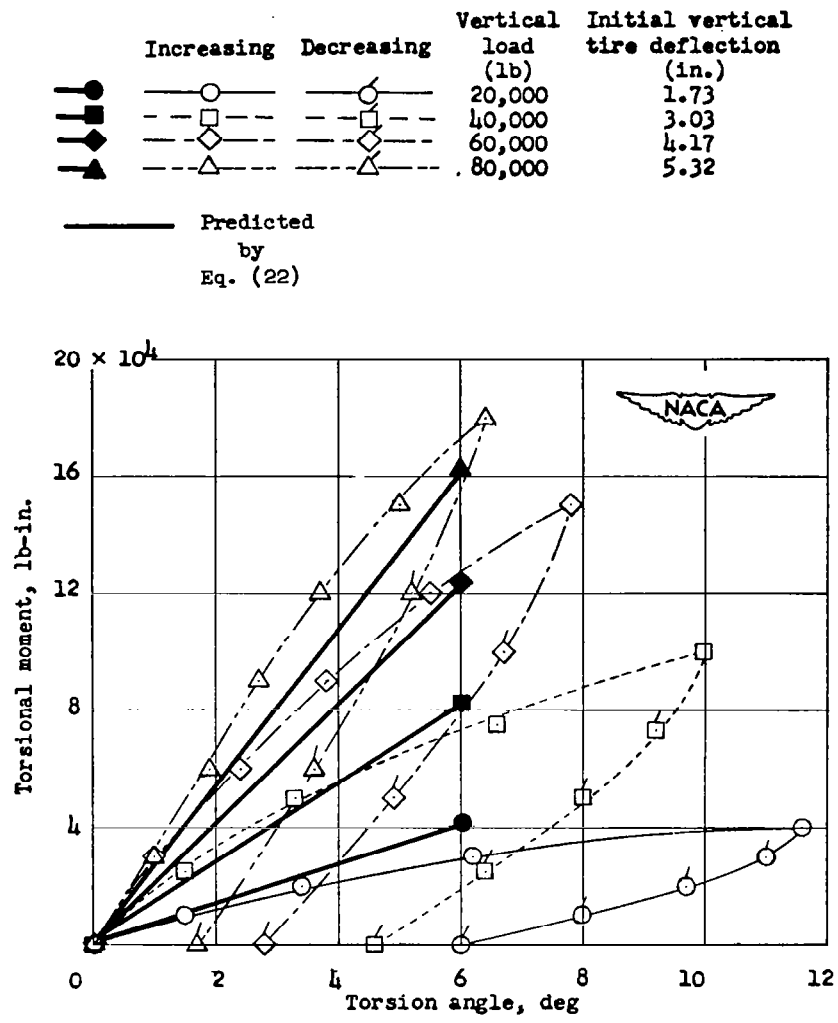


(a) Initial inflation pressure, 200 pounds per square inch.

Fig. 29. Moment-angle of twist experiments vs. predictions of Eq. (22) for tire B.

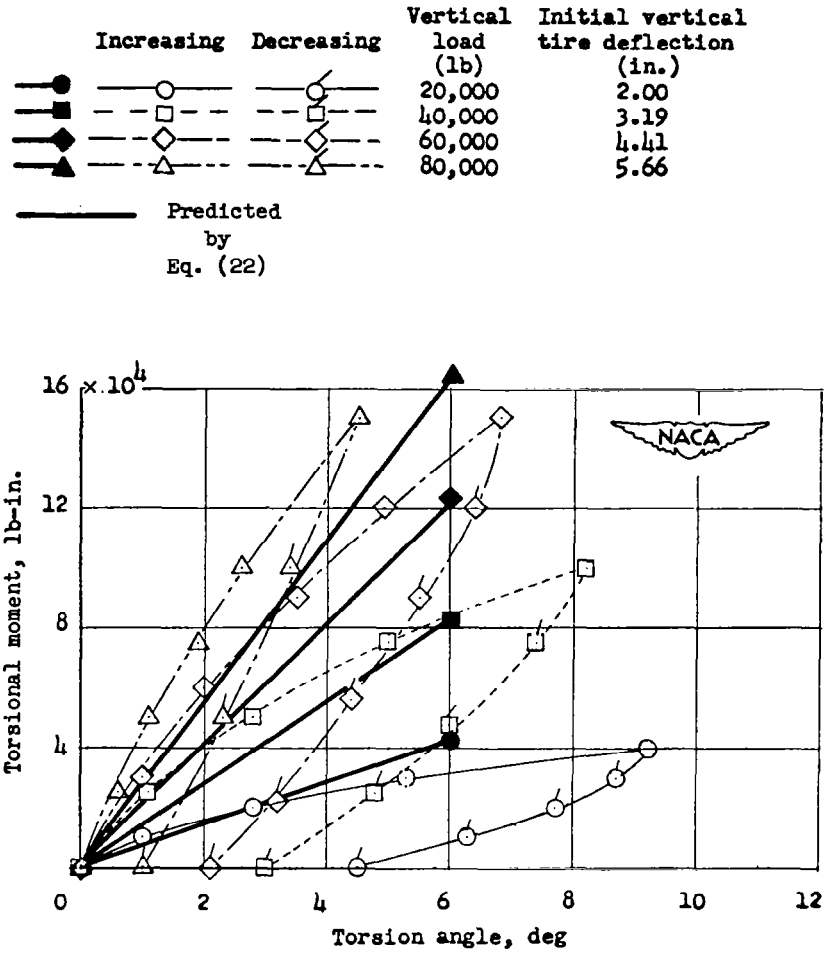


(b) Initial inflation pressure, 180 pounds per square inch.

Fig. 29 (Continued)

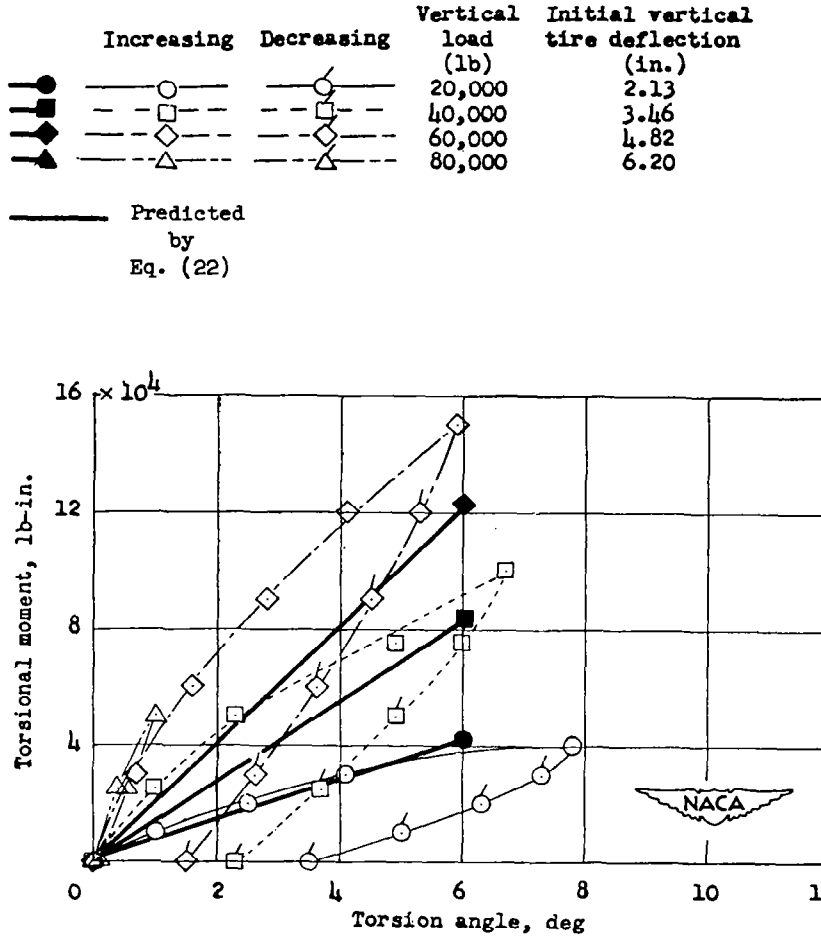


(c) Initial inflation pressure, 160 pounds per square inch.

Fig. 29 (Concluded)

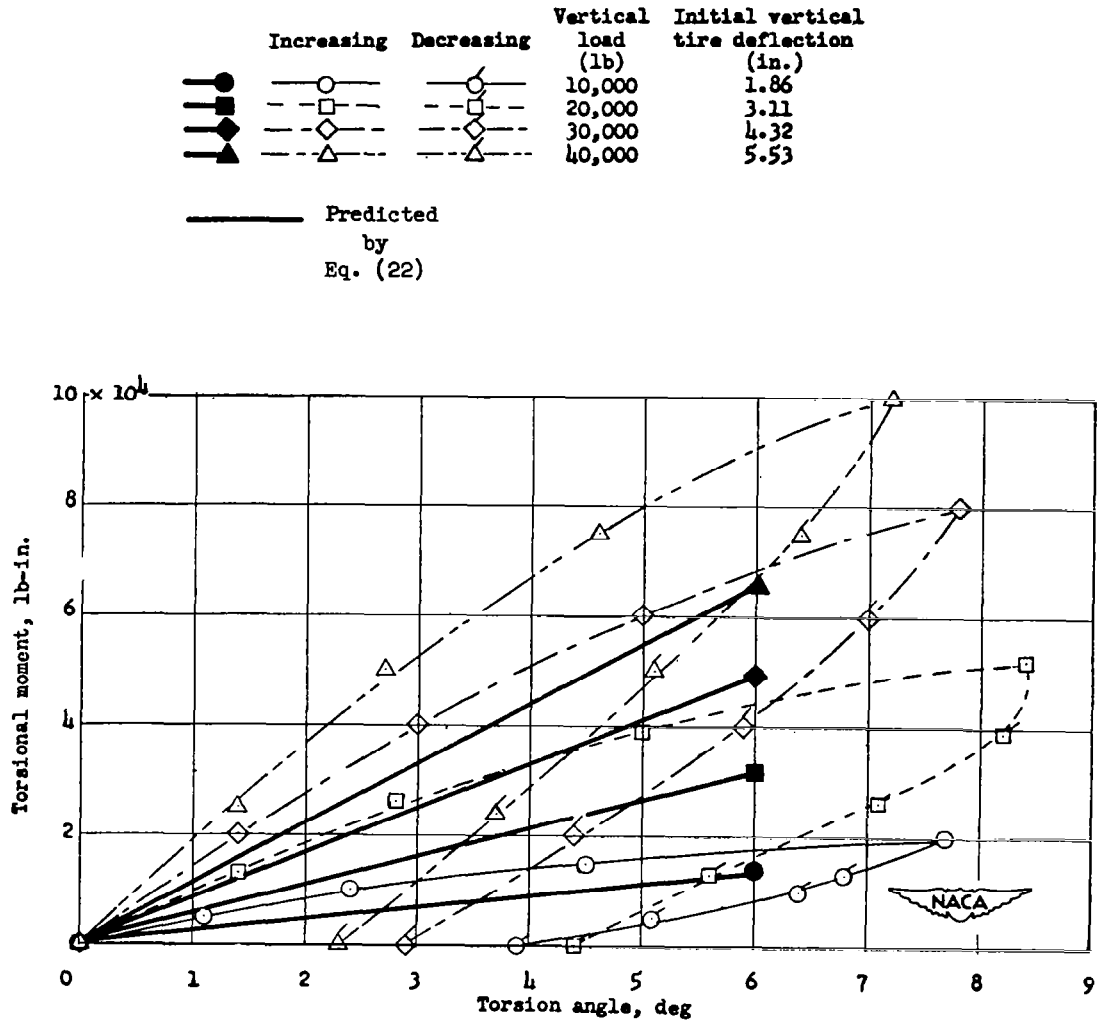


(a) Initial inflation pressure, 105 pounds per square inch.

Fig. 30. Moment-angle of twist experiments vs. predictions of Eq. (22) for tire C.

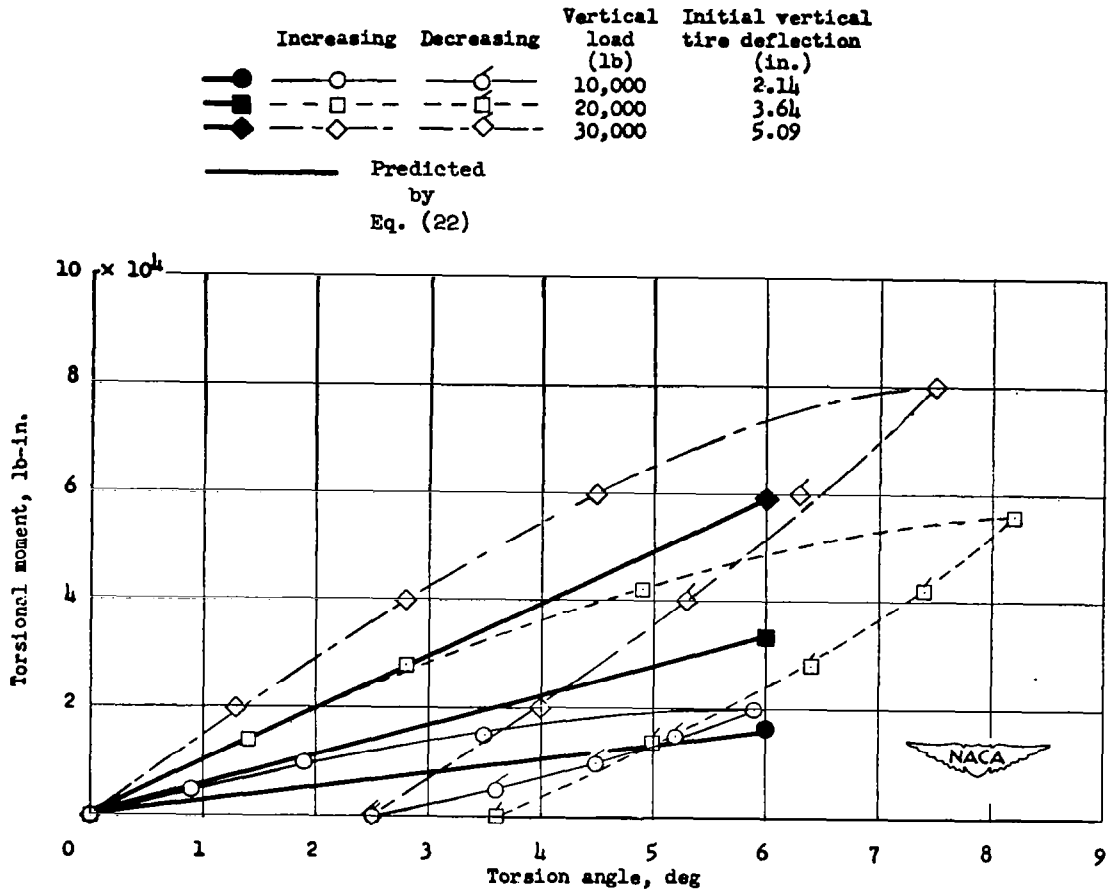


(b) Initial inflation pressure, 85 pounds per square inch.

Fig. 30 (Continued)

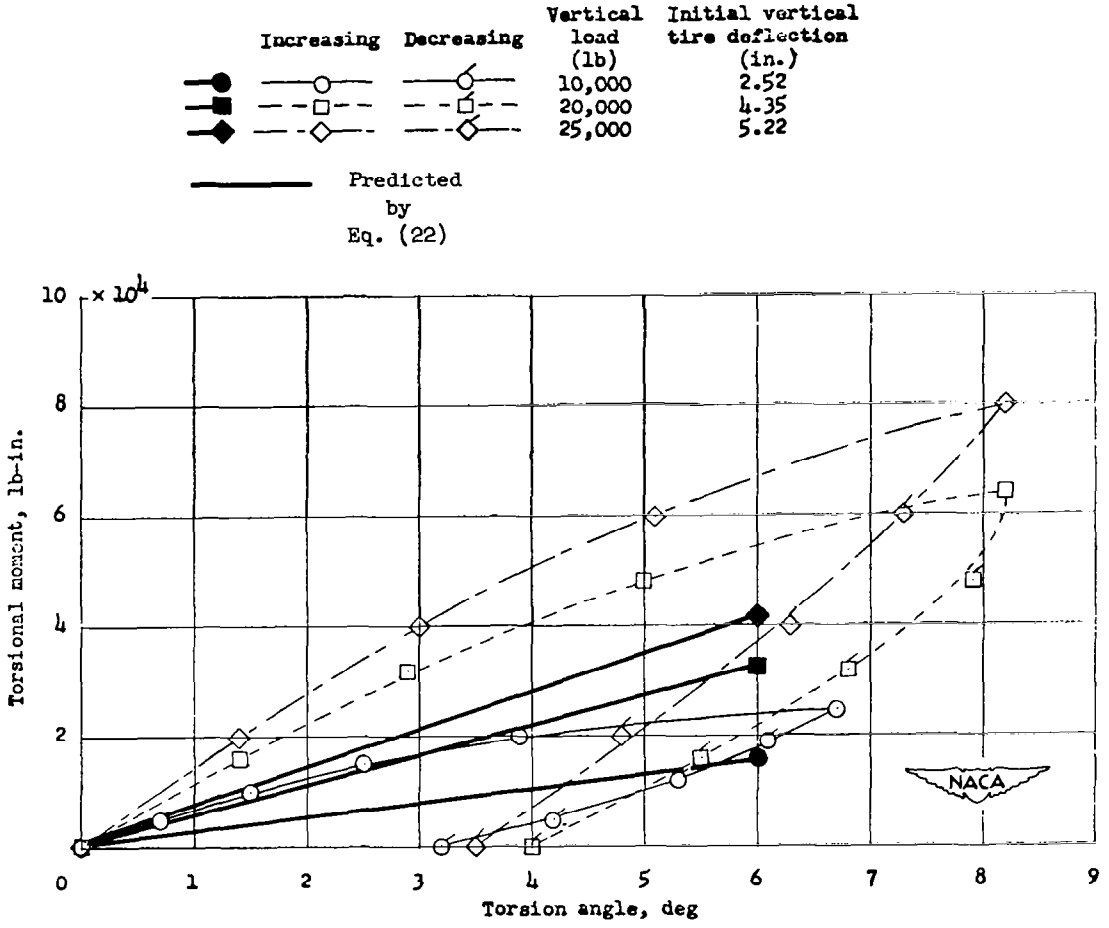


(c) Initial inflation pressure, 65 pounds per square inch.

Fig. 30 (Concluded)

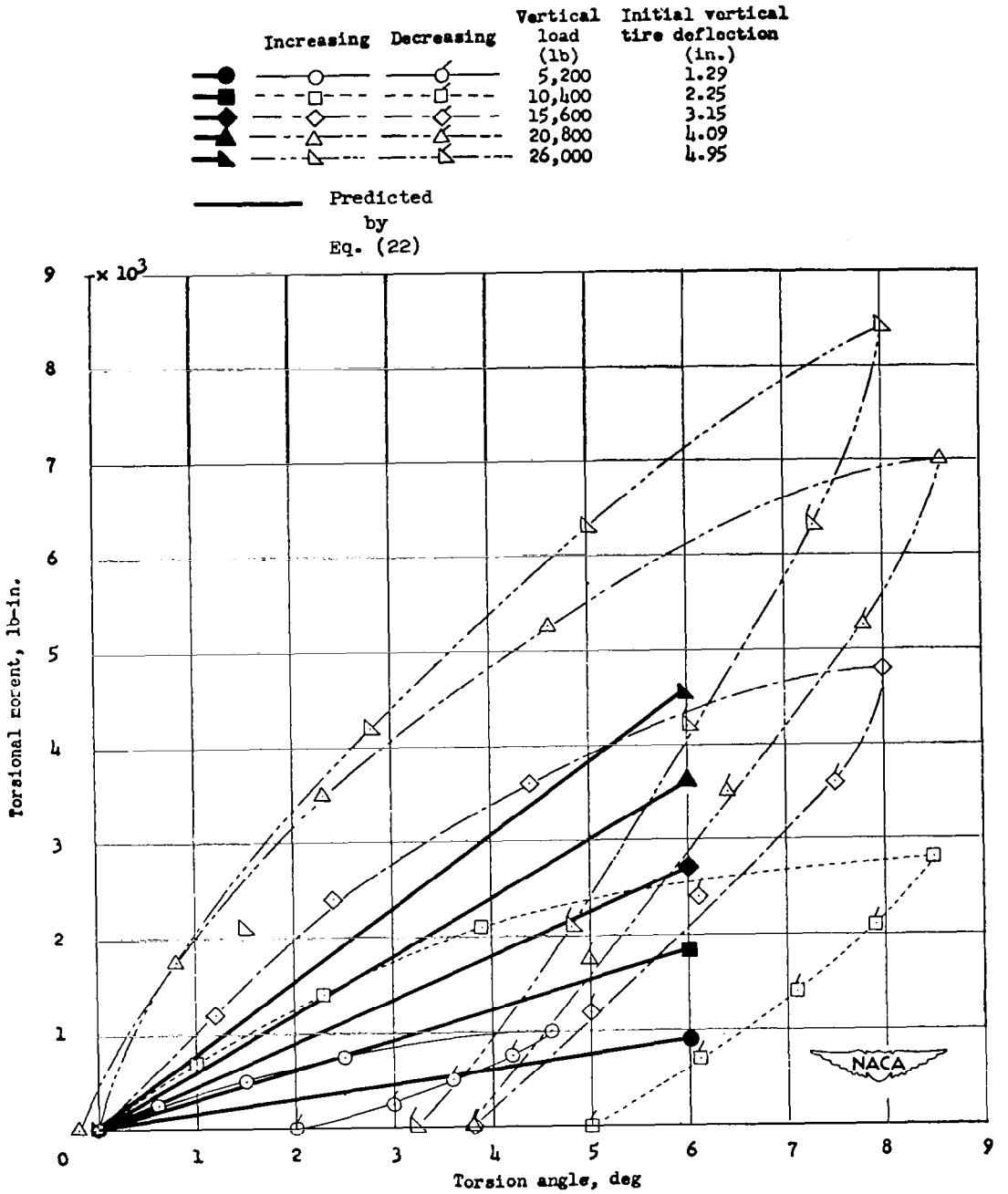


(a) Initial inflation pressure, 75 pounds per square inch.

Fig. 31. Moment-angle of twist experiments vs. predictions of Eq. (22) for tire D.

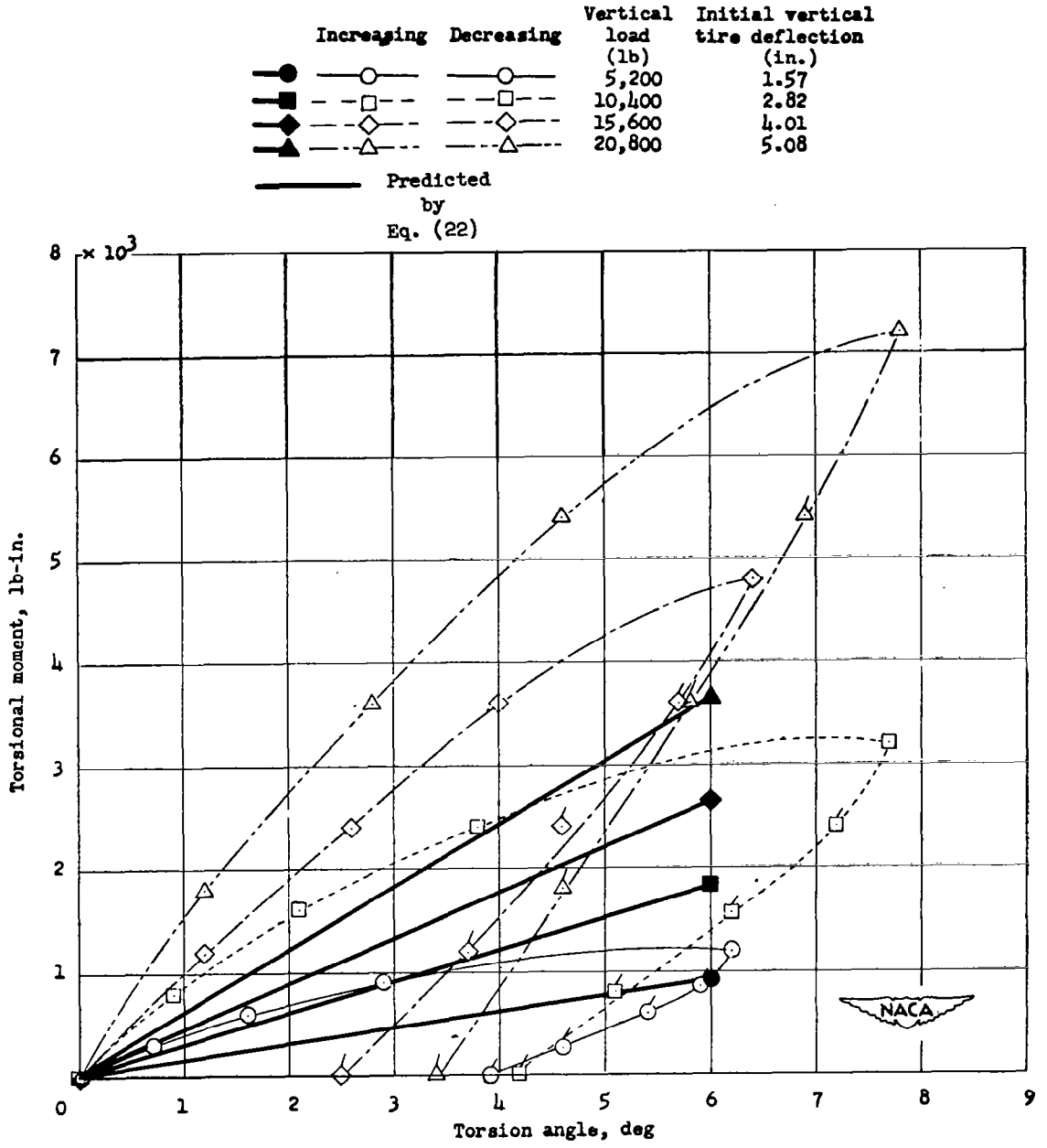


(b) Initial inflation pressure, 55 pounds per square inch.

Fig. 31 (Continued)

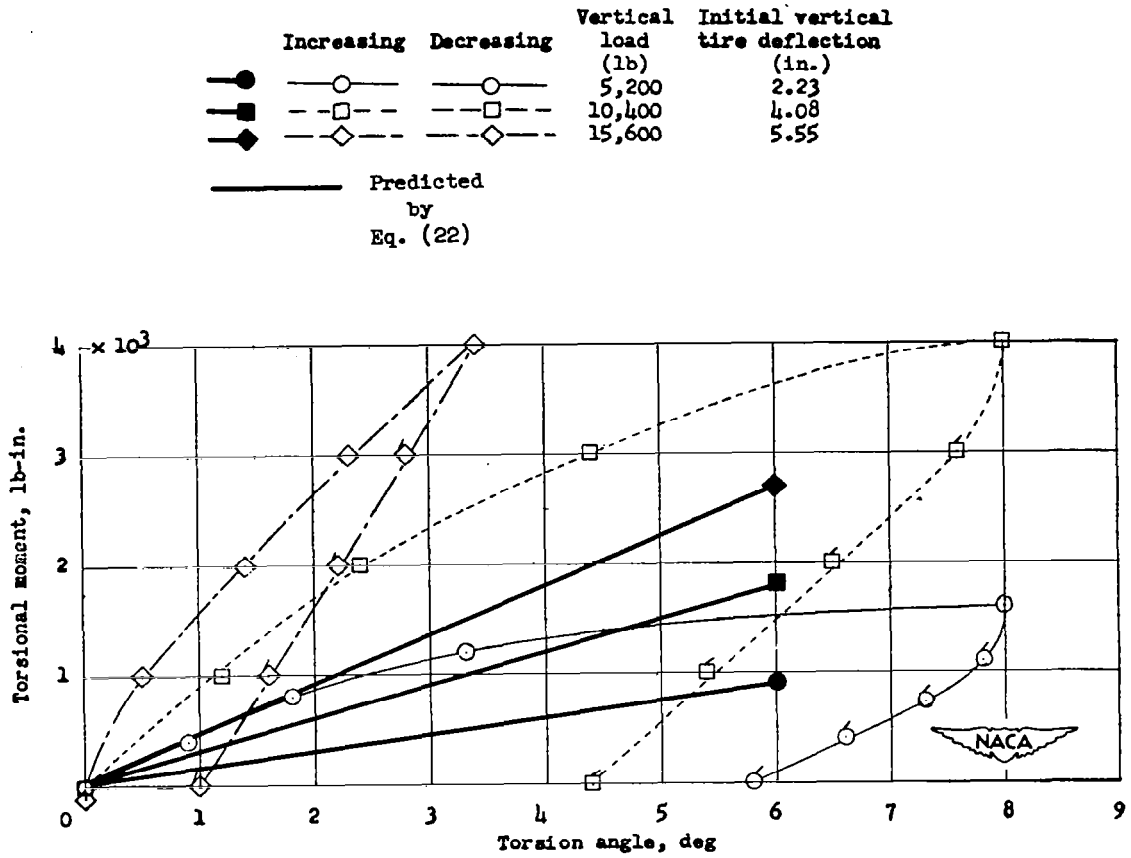


(c) Initial inflation pressure, 35 pounds per square inch.

Fig. 31 (Concluded)

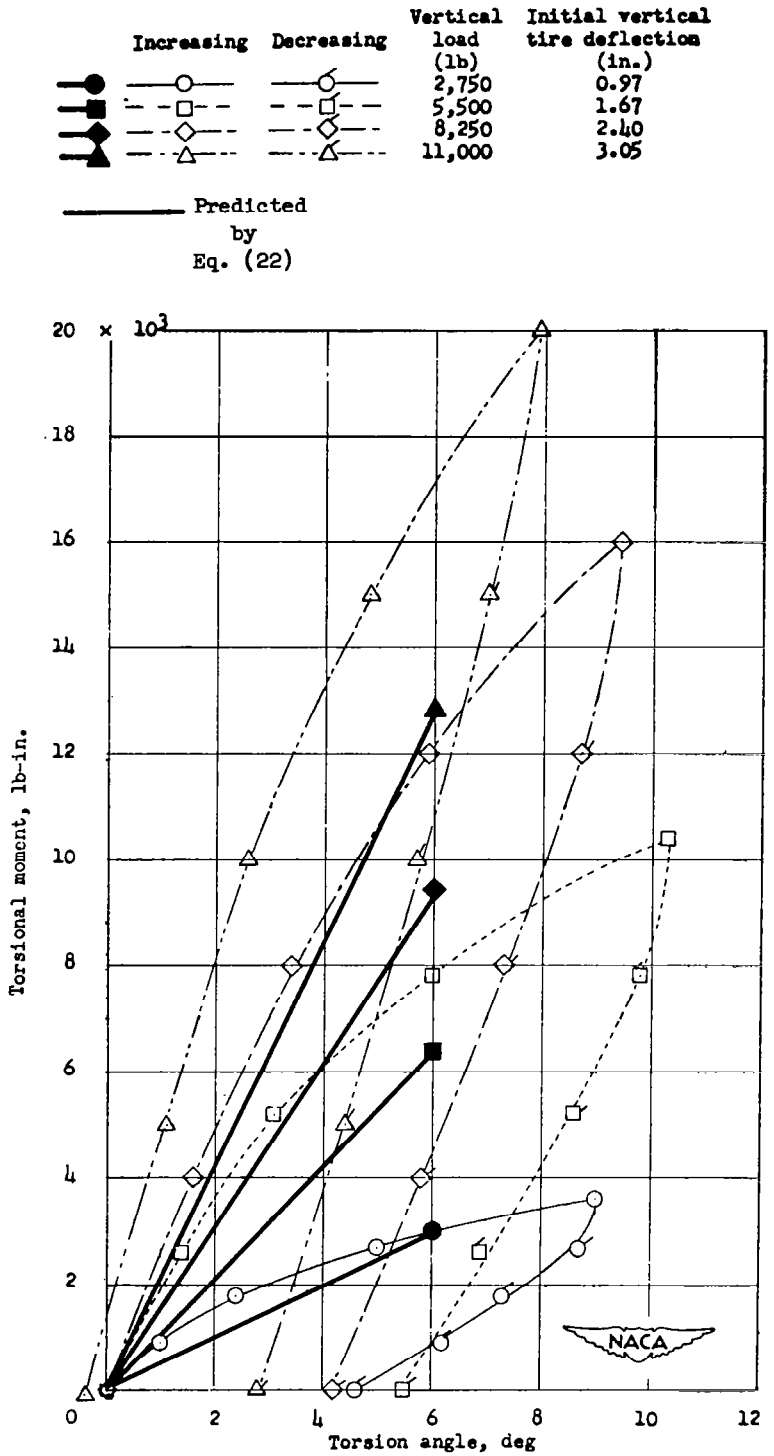


(a) Initial inflation pressure, 80 pounds per square inch.

Fig. 32. Moment-angle of twist experiments vs. predictions of Eq. (22) for tire E.

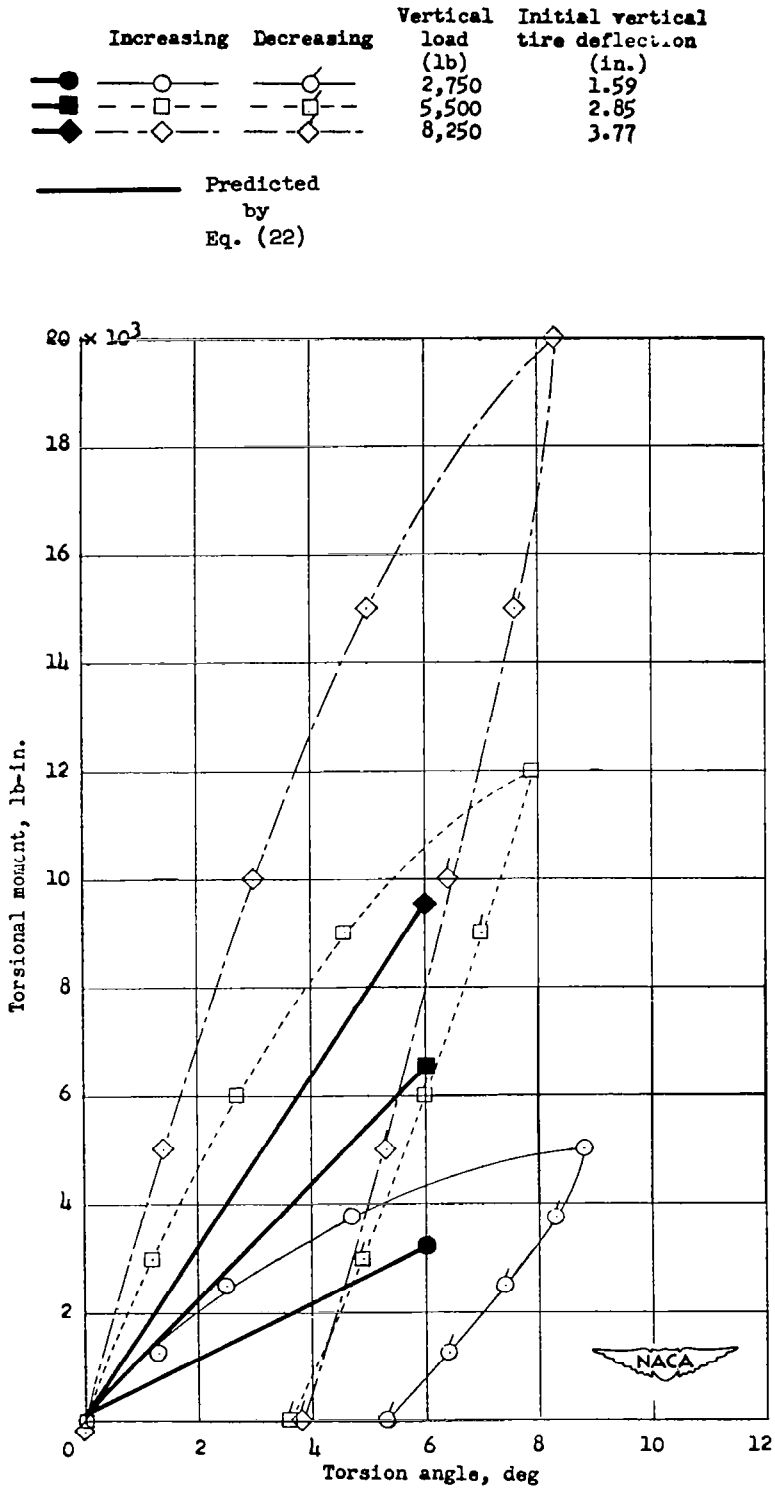


(b) Initial inflation pressure, 40 pounds per square inch.

Fig. 32 (Continued)

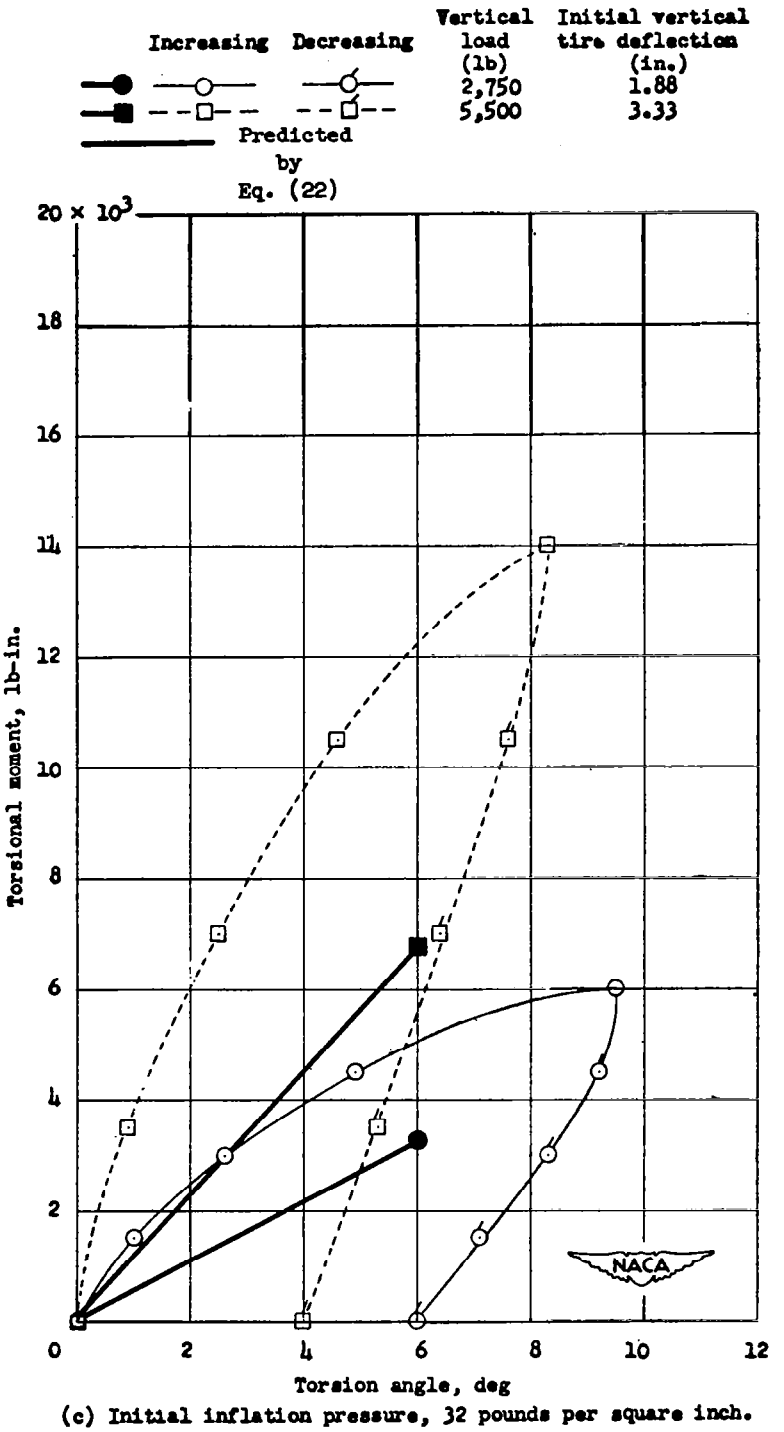


(c) Initial inflation pressure, 32 pounds per square inch.

Fig. 32 (Continued)

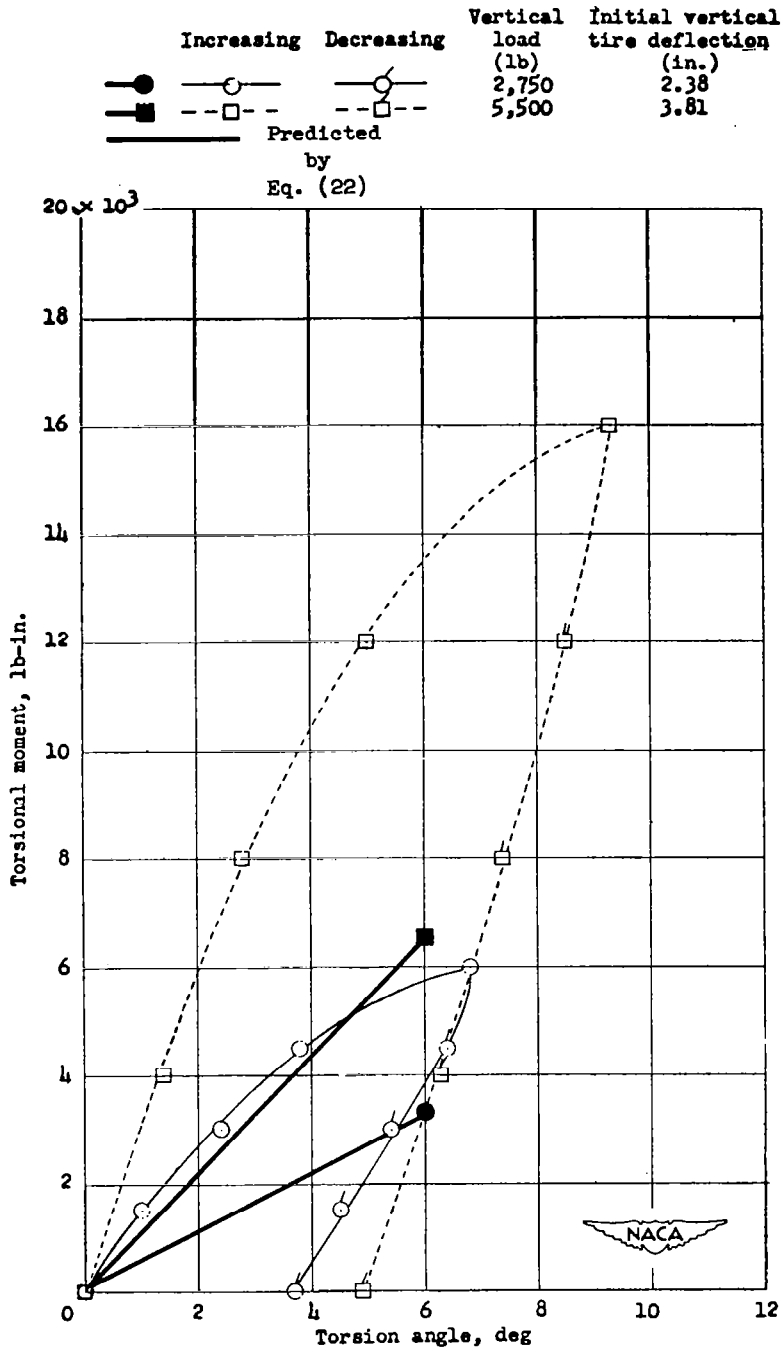


(d) Initial inflation pressure, 24 pounds per square inch.

Fig. 32 (Concluded)